GIScience & Remote Sensing

ISSN: 1548-1603 (Print) 1943-7226 (Online) Journal homepage: www.tandfonline.com/journals/tgrs20

Comparison of GEMS v3.0 tropospheric NO_2 columns with ground-based DOAS instruments in Ulsan

Kangho Bae, Andreas Richter, Kezia Lange, Martina M. Friedrich, Gaia Pinardi, Michel Van Roozendael , Alexis Merlaud, Caroline Fayt, Tim Bösch, Bianca Zilker , Miriam Latsch, Lisa K. Behrens, Hanlim Lee, Yeonjin Jung , Hyunkee Hong , Lim-Seok Chang & Chang-Keun Song

To cite this article: Kangho Bae, Andreas Richter, Kezia Lange, Martina M. Friedrich, Gaia Pinardi, Michel Van Roozendael , Alexis Merlaud, Caroline Fayt, Tim Bösch, Bianca Zilker , Miriam Latsch, Lisa K. Behrens, Hanlim Lee, Yeonjin Jung , Hyunkee Hong , Lim-Seok Chang & Chang-Keun Song (2025) Comparison of GEMS v3.0 tropospheric NO_2 columns with ground-based DOAS instruments in Ulsan, GIScience & Remote Sensing, 62:1, 2597604, DOI: 10.1080/15481603.2025.2597604

To link to this article: https://doi.org/10.1080/15481603.2025.2597604

GISCIENCE & REMOTE SENSING
2025, VOL. 62, NO. 1, 2597604
https://doi.org/10.1080/15481603.2025.2597604

Taylor & Francis
Taylor & Francis Group

RESEARCH ARTICLE

OPEN ACCESS Check for updates

Comparison of GEMS v3.0 tropospheric NO_2 columns with ground-based DOAS instruments in Ulsan

Kangho Bae[a,b], Andreas Richter[c], Kezia Lange[c], Martina M. Friedrich[d], Gaia Pinardi[d], Michel Van Roozendael[d], Alexis Merlaud[d], Caroline Fayt[d], Tim Bösch[c], Bianca Zilker[c], Miriam Latsch[c], Lisa K. Behrens[c], Hanlim Lee[e], Yeonjin Jung[e], Hyunkee Hong[f], Lim-Seok Chang[f] and Chang-Keun Song[a,b,g]

[a]Department of Civil, Urban, Earth and Environmental Engineering, Ulsan National Institute of Science and Technology (UNIST), Ulsan, Republic of Korea; [b]Research & Management Center for Particulate Matters at the Southeast Region of Korea, Ulsan National Institute of Science and Technology (UNIST), Ulsan, Republic of Korea; [c]Institute of Environmental Physics, University of Bremen, Bremen, Germany; [d]Royal Belgian Institute for Space Aeronomy BIRA-IASB, Brussels, Belgium; [e]Division of Earth Environmental System Science, Major of Spatial Information Engineering, Pukyong National University, Busan, Republic of Korea; [f]National Institute of Environmental Research, Incheon, Republic of Korea; [g]Graduate School of Carbon Neutrality, Ulsan National Institute of Science and Technology (UNIST), Ulsan, Republic of Korea

ABSTRACT

This study presents a comprehensive validation of the Geostationary Environmental Monitoring Spectrometer (GEMS) v3.0 tropospheric NO_2 vertical column density (TrVCD) product over Ulsan, South Korea. The evaluation is based on three years of Pandora TrVCDs retrieved from the sky-scan mode measurements at UNIST site (August 2021-July 2024) and two MAX-DOAS instruments operated near emission sources during and after the SIJAQ (Satellite Integrated Joint monitoring of Air Quality) 2022 campaign. Compared with Pandora, GEMS showed fair agreement with a slope of 0.74, a correlation coefficient of 0.55, and a mean relative difference of +46%, generally overestimating at low NO_2 levels but underestimating under high-NO_2 conditions (>1×10^{16} molec. cm^{-2}). To account for spatial representativeness mismatches between GEMS and Pandora, we introduced the Tropospheric Dominance Index (TDI), defined as the ratio between TrVCDs from sky-scan and direct-sun observations. The high-TDI cases (TDI > 85th percentile) exhibited a pronounced negative bias between GEMS and Pandora (MD = -2.67×10^{15} molec. cm^{-2}, MRD = –13.9%), indicating that they were generally associated with GEMS underestimation in high-NO_2 conditions. Seasonal analyses of diurnal variation at UNIST revealed that GEMS exhibited a systematic positive bias but captured similar daily patterns to Pandora in autumn and winter, whereas in spring and summer, the diurnal patterns were less consistent with Pandora. These discrepancies were linked to near-surface advection, with distinctly lower agreement under polluted inflow conditions. Comparisons with MAX-DOAS near emission sources showed lower agreements, with a slope of 0.81 and a correlation coefficient of 0.43, but agreement improved under clean inflow conditions (slope = 1.06, r = 0.59). These results highlight the importance of considering site characteristics and transport conditions in satellite validation and demonstrate the potential of TDI as an auxiliary indicator to identify cases of high NO_2 inhomogeneity and improve future validation strategies for geostationary satellite products.

ARTICLE HISTORY
Received 25 June 2025
Accepted 26 November 2025

KEYWORDS
GEMS; MAX-DOAS; Pandora; validation; diurnal variation

1 Introduction

Nitrogen oxides ($NO_X = NO + NO_2$) are major air pollutants that significantly affect air quality. They are emitted from both natural sources, such as lightning and soil emissions, and anthropogenic activities, including transportation, power plants, and industrial processes (Lamarque et al. 2010; Seinfeld and Pandis 2016). Anthropogenic sources account for the majority of NO_X emissions, especially over densely populated

CONTACT Chang-Keun Song cksong@unist.ac.kr

Supplemental data for this article can be accessed online at https://doi.org/10.1080/15481603.2025.2597604.

and industrial areas. NO_2 poses direct health risks and indirectly contributes to the formation of tropospheric ozone and particulate matter (PM), further deteriorating air quality (Haagen-Smit 1952; Crutzen 1979; Behera and Sharma 2011; Orellano et al. 2020; Meng et al. 2021; Madronich et al. 2023). Due to their high reactivity, NO_X species have a short atmospheric lifetime, typically lasting only a few hours. As a result, NO_2 exhibits pronounced spatial heterogeneity with elevated concentrations near emission sources, and these distributional characteristics provide useful information for identifying source locations and estimating emission fluxes (Beirle et al. 2011; de Foy et al. 2015; Laughner and Cohen 2019). To address the limitations of in-situ observations in spatial coverage, spaceborne NO_2 monitoring systems based on the Differential Optical Absorption Spectroscopy (DOAS; Platt and Stutz 2008) technique have been developed.

Satellite-based air quality monitoring research has primarily relied on Low Earth Orbit (LEO) satellites, such as the Global Ozone Monitoring Experiment–1/2 (GOME–1/2; Burrows et al. 1999; Munro et al. 2006), the Scanning Imaging Absorption Spectrometer for Atmospheric Cartography (SCIAMACHY; Bovensmann et al. 1999), the Ozone Monitoring Instrument (OMI; Levelt et al. 2006), and the TROPOspheric Monitoring Instrument (TROPOMI; Veefkind et al. 2012), which provide global coverage. However, these satellites are limited to observing a target region only once or twice a day. To overcome this limitation, geostationary (GEO) environmental satellite missions have recently been initiated, starting with the Geostationary Environmental Monitoring Spectrometer (GEMS; Kim et al. 2020b) from South Korea, launched in February 2020, followed by the Tropospheric Emissions: Monitoring of Pollution (TEMPO; Zoogman et al. 2017) from the United States launched in April 2023, and European Sentinel–4 (Gulde et al. 2017) launched in July 2025. In contrast to LEO sensors, GEO instruments operate with fixed viewing geometry and under more extreme solar zenith angle conditions, which can introduce unique error characteristics not encountered in LEO observations. Therefore, comprehensive validation with ground-based measurements is essential to assess the quality of GEO retrieval algorithms and guide potential improvements.

Kim et al. (2023b) conducted a validation of the GEMS L2 v1.0 NO_2 total column density (TotVCD) data using Pandora measurements from four different monitoring sites in Seosan, South Korea, between December 2020 and January 2021. Their results showed a correlation coefficient (r) ranging from 0.62 to 0.78 between GEMS and Pandora data, with GEMS underestimating compared to Pandora observations. The evaluation of the GEMS L2 v2.0 NO_2 tropospheric vertical column density (TrVCD) product was conducted by Lange et al. (2024) using Pandora and Multi-Axis Differential Optical Absorption Spectroscopy (MAX-DOAS) observations in the Seoul Metropolitan Area (SMA) and southeastern region of South Korea, from October 2021 to October 2022. The study reported that the GEMS L2 v2.0 NO_2 TrVCD product exhibited fair agreement with ground-based measurements, with a correlation coefficient of 0.75, but GEMS tended to overestimate, showing a median relative bias of +64%. Additionally, the GEMS L2 v2.0 NO_2 TotVCD product was evaluated by Bae et al. (2025) using six Pandora stations across South Korea from October 2021 to November 2022. The study reported that GEMS overestimated compared to ground-based measurements, with a mean relative difference of +41%. This overestimation was more pronounced under high-NO_2 conditions, particularly in the SMA, noontime peaks, and in the winter season. Recent campaign-based validations have revealed clear regional characteristics in the performance of the GEMS v2.0 NO_2 products. Under high-NO_2 conditions ($>1 \times 10^{16}$ molec. cm^{-2}), Lange et al. (2024) and Bae et al. (2025) showed that GEMS systematically overestimated the NO_2 TrVCD compared to both Pandora and MAX-DOAS in the SMA. In contrast, the southeastern cities Busan and Ulsan displayed an underestimation relative to the ground-based instruments. The authors attributed this contrast to sub-pixel inhomogeneity driven by regional transport from sources. These findings highlight the necessity of a dedicated investigation into how regional transport affects the validation performance over the main cities in southeastern Korea.

The aforementioned GEMS validation studies have been campaign-based, providing data sets that span only a few months to a single year. Such limited temporal coverage is not sufficient to fully capture inter-annual variability or season-dependent bias. Therefore, a comprehensive evaluation using a multi-year record of continuous Pandora and MAX-DOAS measurements at a single site is indispensable for establishing reliability by verifying long-term stability of the upgraded GEMS algorithm.

In this study, the GEMS L2 v3.0 NO_2 TrVCD product is validated over a three-year period (August 2021—July 2024) using continuous Pandora measurements at the UNIST site in Ulsan and complementary MAX-DOAS observations collected near major emission sources during, and immediately after, the Satellite Integrated Joint monitoring of Air Quality (SIJAQ) 2022 campaign. Taking advantage of Pandora's

simultaneous observations through different viewing geometries, we suggest a Tropospheric Dominance Index (TDI) to serve as a qualitative flag for highly inhomogeneous conditions. In addition, Automated Synoptic Observing System (ASOS) wind observation data were used to evaluate how wind direction and speed affect the diurnal pattern of NO_2 and influence the validation statistics at each measurement site.

The instruments and datasets used in this study, as well as the co-location criteria, validation statistics, and the TDI are described in Section 2. Section 3 is divided into four parts. Section 3.1 presents the overall three-year validation and yearly comparison between the GEMS v3.0 NO_2 TrVCD and Pandora. Section 3.2 analyses the impact of highly inhomogeneous cases on the validation results by classifying with the TDI. Section 3.3 investigates the season-resolved diurnal patterns of NO_2 TrVCD observed by Pandora and GEMS over the three years and evaluates the influence of wind direction. Section 3.4 provides an additional validation of GEMS with MAX-DOAS observations deployed near emission sources during the SIJAQ2022 campaign and discusses how wind conditions affect the comparison. A summary and conclusions are given in Section 4.

2 Data and methods

Ulsan is one of the largest industrial cities in the Republic of Korea, with a population of more than one million. Ulsan hosts the Hyundai automobile factory, heavy industries, and petrochemical complexes located in the eastern coastal area. Except in the eastern part, Ulsan is surrounded by mountains, and as a result, a steep NO_2 gradient is observed (see Figure 1). Such distinct socio-geographical characteristics of Ulsan make it a suitable location for investigating the spatial representativeness mismatch between coarse-resolution satellite pixels and localized ground-based measurements. In addition, continuous Pandora observations at UNIST over three years provide a valuable dataset for evaluating the seasonal and diurnal characteristics of GEMS retrievals. Based on these advantages, Ulsan was selected as the target city for the SIJAQ2022 campaign. Although the official campaign period lasted from May to August 2022, the stationary remote sensing instruments in Ulsan continued their observations beyond that timeframe. In particular, the Royal Belgian Institute for Space Aeronomy (BIRA) MAX-DOAS, which could not operate during SIJAQ2022, conducted additional measurements from January to June 2023. All instruments used in this study along with their locations and relevant information are described in Figure 1 and Table 1.

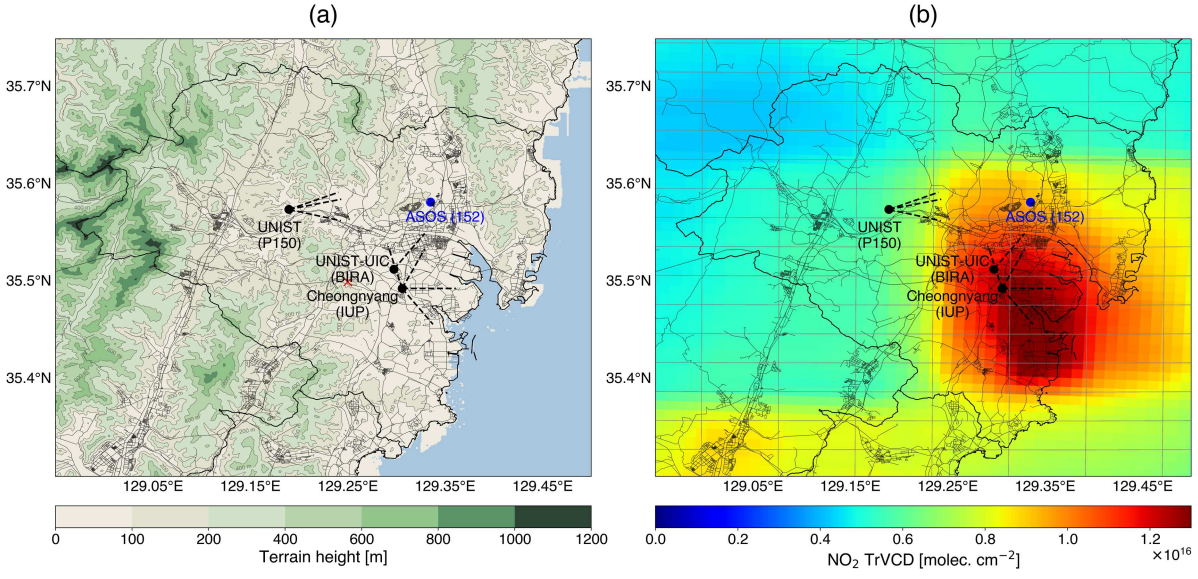

Figure 1. The (a) orographic map and (b) oversampled mean GEMS L2 v3.0 NO_2 TrVCDs for Ulsan from August 2021 to July 2024 at 1 km × 1 km spatial resolution. Black dots show the locations of the ground-based measurement stations, and the blue dot is the location of the ASOS station. Black dashed lines represent the viewing azimuth angles (VAA) in sky-scan mode. The grey line of panel (b) shows the GEMS footprint.

Table 1. List of instruments and their location, observation geometry, VCD retrieval processor, and data period.

Instrument (station acronym)	Location/Platform	Observation geometry	VCD retrieval processor	Period	Viewing azimuth angle (VAA)
GEMS	GK2B		v3.0	Aug. 2021-Jul. 2024	
TROPOMI	S5P		RPRO v2.4.0 OFFL v2.4.0–2.6.0	Aug. 2021-Jul. 2024	
Pandora (P150)	UNIST (35.57 N, 129.19E)	Direct-sun Multi-axis	PGN rnvs3.1–8 PGN rnvh3.1–8	Aug. 2021-Jul. 2024	67° (Aug. 2021-Nov. 2021) 76.5° (Nov. 2021-Aug. 2023 105° (Sep. 2023–Jul. 2024)
IUP-UB MAX-DOAS (IUP)	Cheongnyang (35.49 N, 129.31E)	Multi-axis	FRM_4DOAS 01.01 MMF	Jun. 2022-Oct. 2022	25°, 90°, 145°, 349°
BIRA MAX-DOAS (BIRA)	UNIST-UIC (35.51 N, 129.30E)	Multi-axis	FRM_4DOAS 01.01 MMF	Jan. 2023-Jun. 2023	35°

2.1 Gems

GEMS is the first geostationary spectrometer, operating onboard the Geostationary Korea Multi-Purpose Satellite-2B (GK2B), launched in February 2020. GEMS measures radiation in the 200–500 nm range with a spectral resolution of 0.6 nm. It provides column amounts of gaseous air pollutants, including NO_2, O_3, SO_2, HCHO, and CHOCHO, as well as aerosol properties such as Aerosol Optical Depth (AOD) and Aerosol Effective Height (AEH), over the Asian region (5°S–45°N, 75°E–145°E) with an hourly temporal resolution (Kim et al., 2020b). Most products have a spatial resolution of up to 3.5 km × 8 km; however, pixels are co-added for low signal-to-noise ratio products, such as CHOCHO. Depending on solar position, GEMS operates in four scanning modes, providing up to 10 observations per day. The GEMS L2 products can be downloaded from the National Institute of Environmental Research-Environmental Satellite Center (NIER-ESC) website (https://nesc.nier.go.kr/en/html/datasvc/index.do, last access: 23 September 2025).

The operational GEMS L2 NO_2 product is retrieved from GEMS L1B radiance using a DOAS fit in the 432–450 nm fitting window. Through DOAS spectral fitting, the slant column density (SCD) is first retrieved and subsequently converted to VCD using an Air Mass Factor (AMF). The AMF is determined using shape factors derived from vertical NO_2 profiles simulated by the GEOS-Chem chemical transport model (Bey et al. 2001) climatology at a horizontal resolution of 0.25° × 0.3125°, and scattering weights derived from a pre-calculated look-up-table (LUT) generated with the VLIDORT (Spurr 2006) radiative transfer model as a function of solar and viewing geometric angles (solar zenith angle, viewing zenith angle, and relative azimuth angle), surface reflectance, aerosol information, and cloud pressure. The currently released GEMS NO_2 v3.0 product is generated using the following input data: GEMS L2 aerosol (AERAOD) product v2.1, total ozone (O3T) product v2.1, surface reflectance (BSR) product v3.0, and cloud (CLD) product v3.0. Detailed description of DOAS fitting and retrieval settings can be found in the Algorithm Theoretical Basis Document (ATBD; https://nesc.nier.go.kr/en/html/satellite/doc/doc.do, last access: 23 September 2025).

Retrievals with FinalAlgorithmFlags equal to 0 and CloudFraction less than 0.33 were used to exclude low-quality and cloudy pixels, same as the previous validation studies (Lange et al. 2024; Edwards et al. 2024).

2.2 TROPOMI

TROPOMI is a nadir-viewing grating spectrometer onboard the sun-synchronous Sentinel–5 Precursor (S5P) satellite, launched by the European Space Agency (ESA) in October 2017 to monitor atmospheric air quality (Veefkind et al. 2012). TROPOMI observes ultraviolet (270–329 nm), visible (310–500 nm), near-infrared (675–775 nm), and shortwave-infrared (2305–2385 nm) spectral regions. With a nominal footprint of approximately 3.5 km × 5.5 km at nadir, TROPOMI provides one to two overpasses per day at mid latitudes. During the study period, TROPOMI provided observations over Ulsan between 12:29 and 14:25 KST.

TROPOMI NO_2 TrVCD products are retrieved using the DOAS method applied to the 405–465 nm spectral window (van Geffen et al., 2022). The retrieval involves the separation of stratospheric and tropospheric components based on TM5-MP model profiles and radiative transfer calculations of AMF (Eskes and

Eichmann, 2023). Surface reflectance is based on the directionally dependent Lambertian equivalent reflectivity (DLER) climatology (Tilstra et al. 2024), and cloud parameters are derived using the FRESCO-wide algorithm.

In this study, both the offline (OFFL) and reprocessed (RPRO) datasets generated with processor version 02.04.00 and later were used. These datasets are freely available from the Copernicus Data Space Ecosystem (https://browser.dataspace.copernicus.eu/; last access: 16 October 2025). To ensure data quality, only pixels with a qa_value greater than 0.75 were retained, following the recommendation of Eskes and Eichmann (2023).

2.3 Pandora

The Pandora is a passive ground-based remote sensing instrument equipped with a commercial Avantes spectrometer covering a spectral range of approximately 280–530 nm. Pandora instruments can operate two observation routines, direct-sun (DS) and sky-scan (SS) modes. The DS mode is designed for retrieving TotVCDs by tracking the sun during measurements, with a precision of approximately 0.01 DU (1 DU = 2.69×10^{16} molec. cm^{-2}) and a systematic uncertainty of ~0.1 DU under clear-sky conditions (Herman et al. 2009; Zhao et al. 2019). In contrast, the SS mode retrieves TrVCDs and surface concentrations by scanning at multiple elevation angles along a fixed azimuth direction. At the UNIST site, the fixed viewing directions used in the SS mode (67°, 76.5°, and 105°) varied depending on the operational period, as summarized in Table 1. These viewing directions correspond to major emission source sectors in Ulsan, including petrochemical industrial complexes, dense residential areas, and the Hyundai automobile factory, as shown in Figure 1.

While SS products are still undergoing validation, the CINDI–2 intercomparison showed that the Pandora SS measurements exhibited good agreement with the median of MAX-DOAS instruments, with a bias of approximately -0.02×10^{16} molec. cm^{-2} for the NO_2 TrVCDs under various atmospheric conditions (Tirpitz et al. 2021; Verhoelst et al. 2021). Pandora provides high-frequency measurements in DS mode, with retrievals typically available at sub-minute intervals, whereas SS mode produces TrVCDs approximately every 10 minutes.

The observed radiance spectra in both observation modes are processed into column densities of trace gases, such as NO_2, SO_2, and HCHO, using a centralized algorithm on the Pandonia-Global-Network (PGN; https://www.pandonia-global-network.org, last access: 23 September 2025) server, and are released to the public. In this study, PGN official L2 NO_2 TotVCD and TrVCD products retrieved from P150 (Ulsan, UNIST) observations were used. The location and observation period of the instrument are summarized in Table 1. Detailed descriptions of each product including the DOAS settings can be found in Herman et al. (2009) and Cede (2024). The PGN official algorithm products are labeled with quality flags indicating the retrieval quality as high (0), medium (1), or low (2). Only high and medium quality data were used, including both assured and not assured categories (flags 0, 1, 10, 11).

2.4 MAX-DOAS

As part of the SIJAQ2022 campaign, the Institute of Environmental Physics in Bremen (IUP-Bremen) and the BIRA conducted MAX-DOAS observations in Ulsan in 2022 and 2023, respectively. The IUP-Bremen MAX-DOAS instrument, equipped with a UV spectrometer, is capable of both azimuthal and elevation scanning using a two-dimensional scanner. This setup allowed elevation scanning observations at four different viewing azimuth angles (25°, 90°, 145°, and 349°). These directions cover distinct local environments around the site, ranging from the downtown district (25°) to the petrochemical industrial complex (90°), the Onsan industrial area (145°), and the suburban sector to the north (349°). Since the IUP-Bremen instrument operates only in the UV range, the DOAS fitting was conducted in the UV band, which may lead to a slight underestimation of the differential slant column density (dSCD) retrievals compared to Vis band fitting results due to the shorter effective light path in the UV. BIRA installed the Airyx Compact Skyspec MAX-DOAS (https://airyx.de/wp-content/uploads/2025/05/SkySpec-Compact.pdf, last access: 23 September

2025), which operates with an Avantes spectrometer covering the 300–460 nm spectral range. The elevation angle is adjusted using a 180° rotating prism, allowing for elevation scans in two azimuthal viewing directions. However, in this study, the retrieval from the Airyx Compact SkySpec MAX-DOAS was performed only at a single viewing azimuth angle (35°) due to obstructions. This 35° viewing direction is oriented toward a residential area, which is similar to the 25° azimuthal direction used by the IUP-Bremen instrument. Both the IUP-Bremen and BIRA-IASB MAX-DOAS instruments produced TrVCD data with a temporal resolution of approximately 10 minutes per full elevation scan.

Data from both instruments were analyzed using the centralized FRM$_4$DOAS framework (https://frm4doas.aeronomie.be/, last access: 24 September 2025), utilizing the QDOAS software (Danckaert et al. 2017) to retrieve differential slant column densities (dSCDs), which were subsequently used to derive tropospheric VCDs through the Mexican MAX-DOAS Fit (MMF; Friedrich et al. 2019) inversion algorithm. The MMF algorithm employs an optimal estimation approach with a comprehensive uncertainty budget. Friedrich et al. (2019) reported total uncertainties of approximately 14–20% for NO_2 TrVCDs, comprising smoothing errors (12.5%), measurement noise (2.4%), spectroscopic uncertainties (3.0%), and aerosol extinction profile uncertainties (5.1–9.8% depending on O_4-based aerosol retrieval). The FRM$_4$DOAS framework provides quality flags separately from the MMF algorithm and the Mainz Profile Algorithm (MAPA; Beirle et al. 2019), as well as combined quality flags integrating both algorithms. In this study, the MAX-DOAS dataset was filtered using the overall quality flag (qa_flag_no2) with only "okay" (0) and "warning" (1) data retained. A detailed description of the FRM$_4$DOAS system can be found in Van Roozendael et al. (2024).

2.5 Wind data

To investigate the transport characteristics of NO_2 TrVCDs of Ulsan, wind data were obtained from the ASOS observation data. The ASOS network, operated by the Korea Meteorological Administration (KMA), is maintained in accordance with the guidelines of the World Meteorological Organization (Jarraud 2008). In this study, hourly wind speed and direction from the nearest ASOS station were used and temporally interpolated to the GEMS observation times. The location of the nearest ASOS station is shown in Figure 1.

2.6 Co-location criteria and validation statistics

Coincident measurements were defined by selecting the GEMS pixel containing the observation site and averaging the ground-based stationary measurements within ±30 minutes of the GEMS observation time. Sensitivity tests were performed to evaluate the effects of the averaging time window and the co-location distance measured along the instruments' fixed viewing direction when selecting GEMS pixels for co-location. These results, shown in Figure A1, were either worse or not significantly better than the simple approach using the station containing pixel and ±30-minute window. The insensitivity of the correlation coefficients to the co-location window size is due to the good autocorrelation of the Pandora NO_2 TrVCDs ($r = 0.88$ even at a 30-minute lag; see Figure A1e), which indicates that observations within ±30 minutes generally maintain stable temporal coherence. Validation results are described using a linear regression by a Reduced Major Axis (RMA; Clarke 1980), as well as the Pearson correlation coefficient (r). RMA regression was chosen instead of ordinary least-squares regression because the ground-based reference measurements also involve uncertainties, and RMA accounts for errors in both variables (Boersma et al. 2009; Judd et al. 2020). Additionally, the mean difference (MD), mean absolute difference (MAD), and mean relative difference (MRD), together with their standard errors (SE), are calculated using the following equations:

$$MD = \frac{1}{N}\sum_{i=1}^{N}\left(VCD_{GEMS,i} - VCD_{REF,i}\right) \tag{1}$$

$$MRD = \frac{1}{N}\sum_{i=1}^{N}\left(\frac{VCD_{GEMS,i} - VCD_{REF,i}}{VCD_{REF,i}}\right) \times 100\% \tag{2}$$

$$MAD = \frac{1}{N}\sum_{i=1}^{N}\left|\left(VCD_{GEMS,i} - VCD_{REF,i}\right)\right| \quad (3)$$

$$SE = \frac{\sigma}{\sqrt{N}} \quad (4)$$

Where ***N*** and ***σ*** represent the number of data and the standard deviation, respectively. The reference measurements (REF) are ground-based instruments, either Pandora or MAX-DOAS, as described in Table 1.

2.7 Tropospheric dominance index (TDi)

In principle, NO_2 TotVCD includes both the stratospheric and tropospheric components and should therefore always be larger than the NO_2 TrVCD. However, as shown in Figure 2a, there are cases where the NO_2 TrVCD retrieved from the SS mode ($TrVCD_{SS}$) exceeds the NO_2 TotVCD derived from the DS mode ($TotVCD_{DS}$) from the P150 Pandora instrument. One possible reason for these cases is the difference in observation geometry between the two modes, which makes the SS mode characterized by a longer horizontal representativeness than the DS mode. In DS mode, the horizontal absorption path lengths are generally within 4 km when the solar zenith angle is lower than 50° (Herman et al. 2009). In contrast, the SS mode exhibits a longer horizontal representativeness than the DS mode, typically ranging from 3 to 15 km depending on the aerosol loading (Vlemmix et al. 2010; Irie et al. 2011). Considering that the UNIST site is located away from the urban center and shows relatively low NO_2 TrVCDs (see Figure 1), the effective horizontal representativeness is likely shorter than 15 km but still considerably longer than that of the DS mode. As a result, because the SS mode has a longer horizontal representativeness than the DS mode, the SS observations are more influenced by local changes occurring several kilometers away from the measurement site. Consequently, when pollution levels increase in distinct areas along the line of sight of SS observations, the SS mode tends to reflect such changes more than the DS mode, occasionally yielding higher $TrVCD_{SS}/TrVCD_{DS}$ ratios. Based on this characteristic, we aimed to identify spatially heterogeneous cases using the ratio of TrVCDs retrieved from the two observation modes. The TrVCD in the DS mode ($TrVCD_{DS}$) was derived by subtracting the climatological stratospheric vertical column density

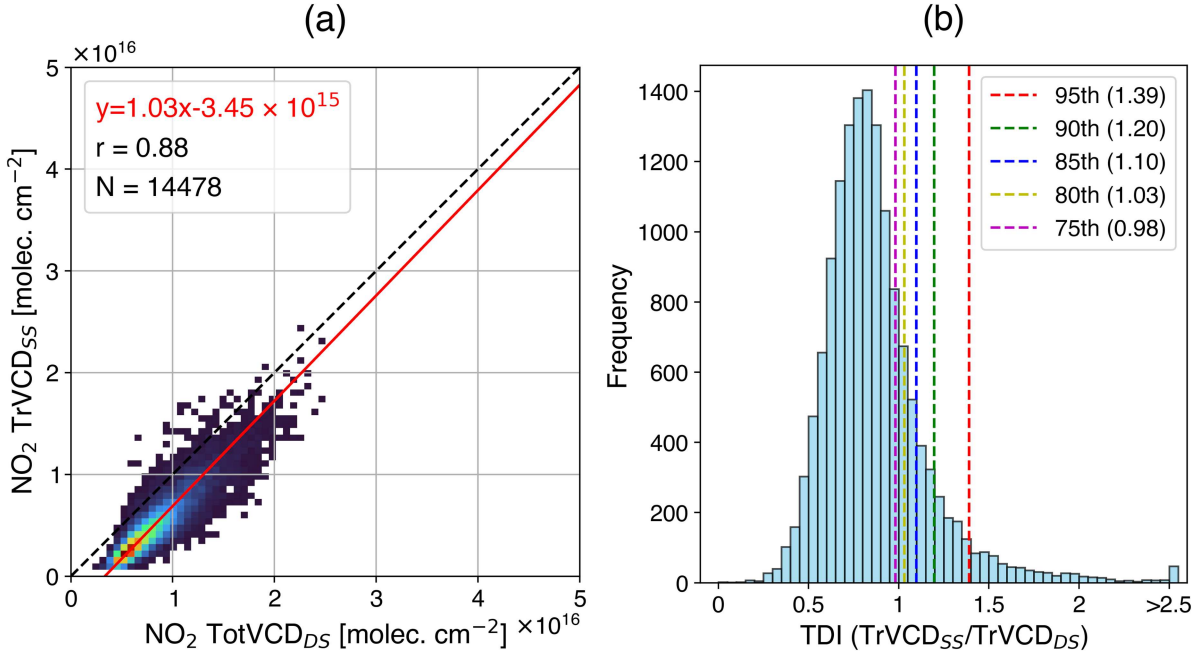

Figure 2. (a) Scatter density plot between $TotVCD_{DS}$ and $TrVCD_{SS}$, and (b) histogram of TDI. Vertical dashed lines in panel (c) indicate the 75th, 80th, 85th, 90th, 95th percentile values.

($StratVCD_{climatology}$), which is provided by the PGN, from the TotVCD. Consequently, the TDI is defined as the ratio between the $TrVCD_{SS}$ and $TrVCD_{DS}$, as shown in Equation 6:

$$TrVCD_{DS} = TotVCD_{DS} - StratVCD_{climatology} \tag{5}$$

$$TDI = \frac{TrVCD_{SS}}{TrVCD_{DS}} \tag{6}$$

3 Results

3.1 Evaluating GEMS NO_2 TrVCD with Pandora

In this section, the GEMS v3.0 NO_2 TrVCD product is compared with Pandora observations at the UNIST site. To ensure consistency with the MAX-DOAS comparison in section 3.4, Pandora TrVCDs retrieved from the SS mode were used in this analysis. Figure 3 presents the three-year time series of NO_2 TrVCDs from Pandora (P150) and GEMS at the UNIST site, covering the period from August 2021 to July 2024. Both Pandora and GEMS exhibit a typical seasonal cycle, with higher values in winter and lower values in summer. In Ulsan, anthropogenic sources such as manufacturing combustion (39%) and energy industry combustion (17%) are the dominant contributors to NO_X emissions, according to the Korean emission inventory from the Clean Air Policy Support System (CAPSS; https://www.air.go.kr/eng/main.do, last access: 23 September 2025). During winter, additional emissions from residential and industrial heating further increase NO_2 concentrations (Lee et al. 2023). Together with reduced solar radiation that weakens photochemical reactions, these enhanced emissions lead to a longer atmospheric lifetime of NO_2, resulting in elevated NO_2 levels during the cold season. In contrast, during summer, enhanced photochemical reactions shorten the atmospheric lifetime of NO_2, leading to lower observed columns (Choi et al. 2021; Kim et al., 2020a; Kim et al., 2023a). Considering the monthly median, GEMS generally reports slightly higher values than Pandora, except during the summer months.

For a quantitative comparison, Figure 4 shows the scatter density plots of co-located GEMS and Pandora measurements. The analysis was performed not only for the entire observation period but also for three separate one-year intervals, and the corresponding statistical results are summarized in Table 2. This separation was made to facilitate comparison with the MAX-DOAS results presented in Section 3.4, as well as to assess the retrieval stability in the year-to-year statistics. Over the entire observation period

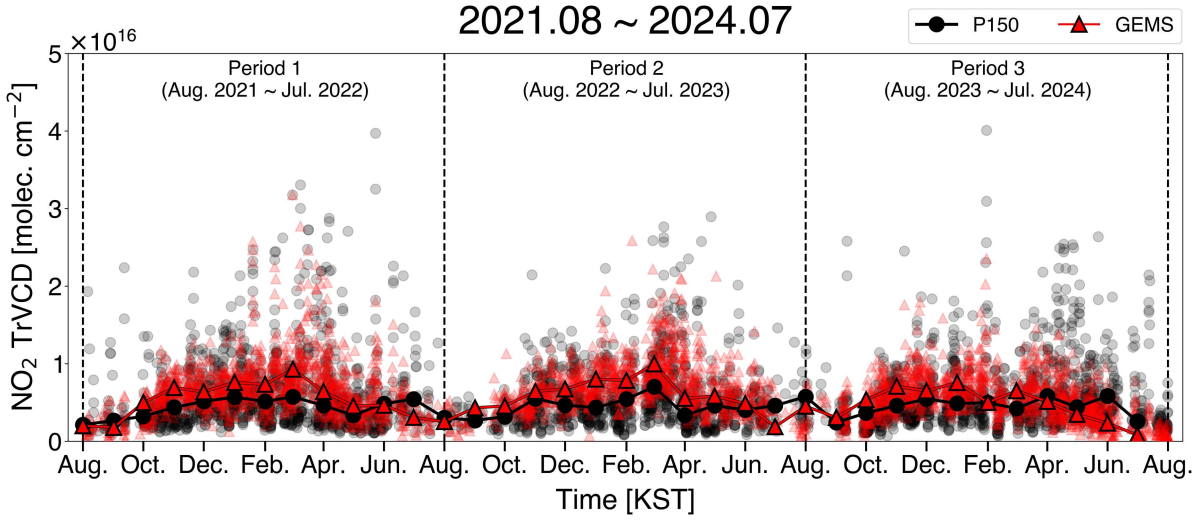

Figure 3. Time series of Pandora and GEMS observations. Semi-transparent dots represent hourly coincident measurements, while solid lines with filled markers indicate the monthly median values.

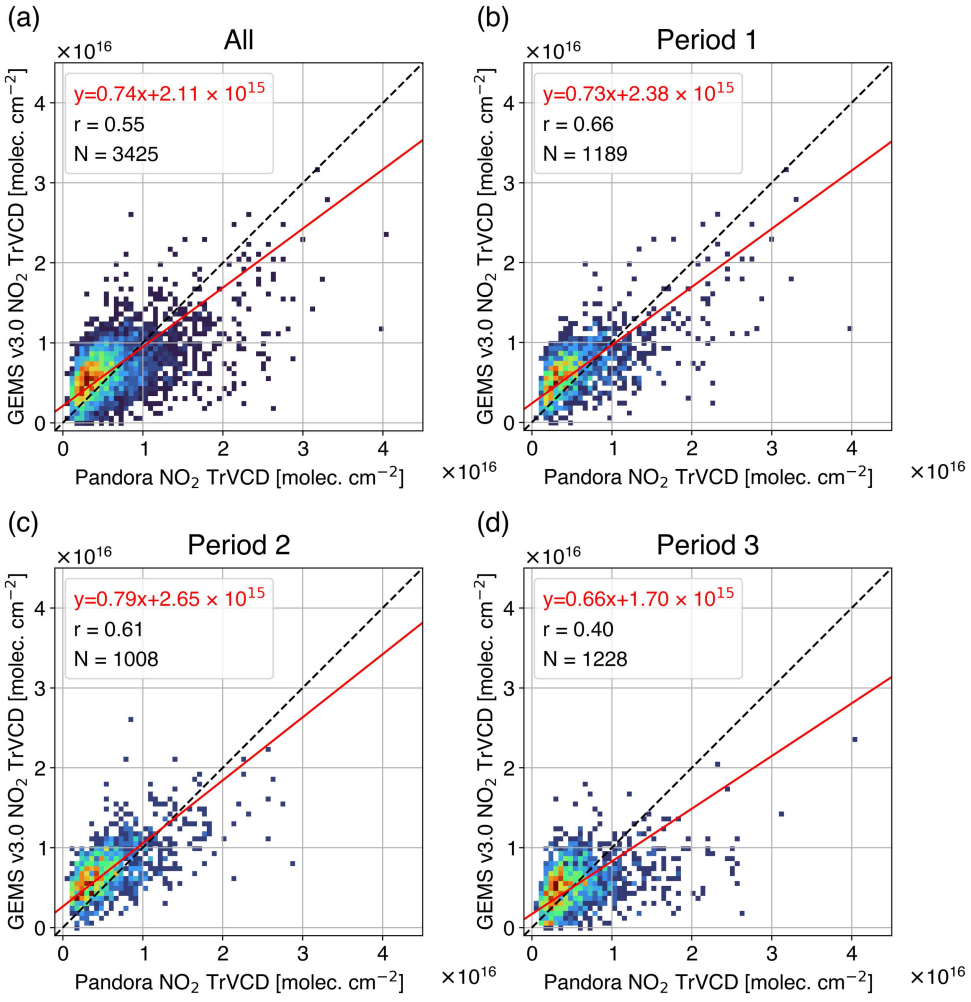

Figure 4. Scatter density plots of Pandora (X-Axis) and GEMSv3.0 (Y-Axis) during (a) entire period, (b) period 1 (August 2021 to July 2022), (c) period 2 (August 2022 to July 2023), and (d) period 3 (August 2023 to July 2024). The red solid line displays the RMA regression result while the black dashed line represents the 1:1 line.

Table 2. GEMS NO_2 TrVCD validation statistics at UNIST (P150). The uncertainty of MD and MRD represents the standard error.

	Slope[a]	y-intercept[b]	MD[c]	MAD[d]	MRD[e]	r[f]	n[g]
All data	0.74	2.11	0.60 ± 0.07	2.91 ± 0.04	45.6 ± 1.6	0.55	3425
Period 1	0.73	2.38	0.74 ± 0.11	2.84 ± 0.07	47.0 ± 2.4	0.66	1189
Period 2	0.79	2.65	1.44 ± 0.11	2.90 ± 0.07	65.1 ± 3.1	0.61	1008
Period 3	0.66	1.70	−0.24 ± 0.12	2.98 ± 0.08	28.2 ± 2.5	0.40	1228
TDI < 85th	0.80	2.12	1.10 ± 0.06	2.70 ± 0.04	54.7 ± 1.7	0.58	2969
TDI > 85th	0.73	−0.02	−2.67 ± 0.25	4.26 ± 0.19	−13.9 ± 2.5	0.51	456

[a]RMA regression slope.
[b]y-intercept of RMA regression (× 10^{15} molec. cm^{-2}).
[c]Mean difference (× 10^{15} molec. cm^{-2}).
[d]Mean absolute difference (× 10^{15} molec. cm^{-2}).
[e]Mean relative difference (%).
[f]Correlation coefficient.
[g]Number of coincident measurements.

(see Figure 4a), the GEMS NO_2 TrVCD exhibits a correlation coefficient of 0.55, a slope of 0.74, an MD of 5.96×10^{14} molec. cm^{-2}, and an MRD of 46%. GEMS v3.0 product continues to overestimate ground-based data when the Pandora NO_2 TrVCD is below 1×10^{16} molec. cm^{-2}, and underestimate it when the TrVCD exceeds this threshold. Compared to the previous GEMS v2.0 performance over the same period (r = 0.51,

slope = 0.62, MD = 3.51 × 10^{15} molec. cm^{-2}; see Figure A2 and Table A1), the improved slope and reduced bias indicate that algorithmic updates have enhanced the agreement with Pandora observations. This improvement can be attributed to several key updates implemented in the GEMS v3.0 retrieval algorithm. The correction of errors in the shape-factor calculation derived from a priori NO_2 profiles, the update of the tropopause pressure of 230 hPa, which mitigated the unrealistic stratospheric columns observed in v2.0, and the improvement of GEMS L2 auxiliary data products including aerosol (AERAOD), total ozone (O_3T), surface reflectance (BSR), and cloud (CLD) products collectively contribute to a more accurate AMF computation and improved NO_2 column estimates (Lee et al. 2024). In particular, regarding surface reflectance, Lange et al. (2024) demonstrated based on the IUP-UB scientific GEMS NO_2 product that the use of the GEMS BSR v2.0 product resulted in a lower correlation with ground-based measurements than the TROPOMI LER product. Therefore, the update to the GEMS BSR v3.0 dataset likely contributed to the improved agreements with Pandora in the present study. Nevertheless, GEMS v3.0 still shows a positive bias compared to Pandora, and this bias is larger than that found in the TROPOMI comparison (see Figure A3). Several factors may contribute to this higher bias in GEMS. First, due to the geostationary viewing geometry, GEMS retrievals are more sensitive to uncertainties in the AMF under high solar zenith angles, particularly in the morning and evening. These conditions, in combination with enhanced aerosol loads and low boundary layer heights, can amplify retrieval uncertainties, whereas TROPOMI is less affected. Second, unlike TROPOMI, which applies daily a priori NO_2 profiles from a TM5-MP model, GEMS currently relies on monthly climatological a priori information, which can limit the accuracy of the shape factor calculation.

When the annual GEMS NO_2 products are evaluated in individual years, the slope and correlation coefficient in Period 3 (August 2023—July 2024) show reduced agreement compared to those in Period 1 (August 2021—July 2022) and Period 2 (August 2022—July 2023). In particular, the correlation coefficient decreases from 0.66 and 0.61 in Periods 1 and 2, respectively, to 0.40 in Period 3. This decline is attributed to greater underestimation under high-NO_2 conditions (>1 × 10^{16} molec. cm^{-2}) during Period 3 (Figure A3), and is partly associated with meteorological factor that likely enhanced the horizontal smoothing effect.

The horizontal smoothing effect, caused by the mismatch in spatial representativeness between satellite pixels and ground-based instruments, provides an explanation for the satellite underestimation observed under high-NO_2 conditions. Ground-based instruments such as Pandora SS and MAX-DOAS retrieve TrVCDs along a narrow line of sight, whereas satellite observations provide area-averaged TrVCDs over a much larger pixel footprint.

This mismatch gives rise to two types of errors. First, the dilution of localized NO_2 enhancements within the satellite pixel varies from hour to hour with changes in wind conditions and plume position. This variability increases random bias and consequently reduces the correlation between the two datasets. Second, when high-NO_2 plumes are spatially skewed within the pixel—particularly along the line of sight of the ground-based instrument—Pandora tends to sample the plume core, whereas GEMS retrieves a diluted pixel-average value, resulting in a persistent systematic negative bias.

Such horizontal smoothing effects have been consistently reported in previous studies. Herman et al. (2019) showed that OMI underestimated Pandora NO_2 columns by up to 50–100% in polluted urban areas, mainly due to its coarse spatial resolution relative to localized emission plumes. Judd et al. (2019) further confirmed this using airborne GeoTASO (~250 m resolution) together with Pandora observations, demonstrating that coarse-resolution satellite pixels systematically diluted urban NO_2 hotspots and underestimated column densities compared to high-resolution measurements. Likewise, Ialongo et al. (2020) found that TROPOMI underestimated Pandora observations during elevated pollution episodes in Helsinki, attributing the sub-pixel variability. Karagkiozidis et al. (2023) similarly reported that in Thessaloniki, TROPOMI generally underestimates NO_2 columns because satellite pixels average over heterogeneous emission sources. These findings highlight that pixel-scale spatial inhomogeneity is one of the key drivers of discrepancies in satellite-to-ground NO_2 comparisons.

In Period 3, as shown in Figure 5, the relative frequency of northerly winds—which typically represent clean inflow—was substantially lower compared to Period 1 and 2. Conversely, the occurrence of easterly and southerly winds, transporting polluted air masses from the industrial complexes and nearby urban areas, became more dominant. This increased frequency of polluted inflow during Period 3 likely amplified smoothing effects, resulting in stronger random and systematic components of the GEMS bias at the P150 site.

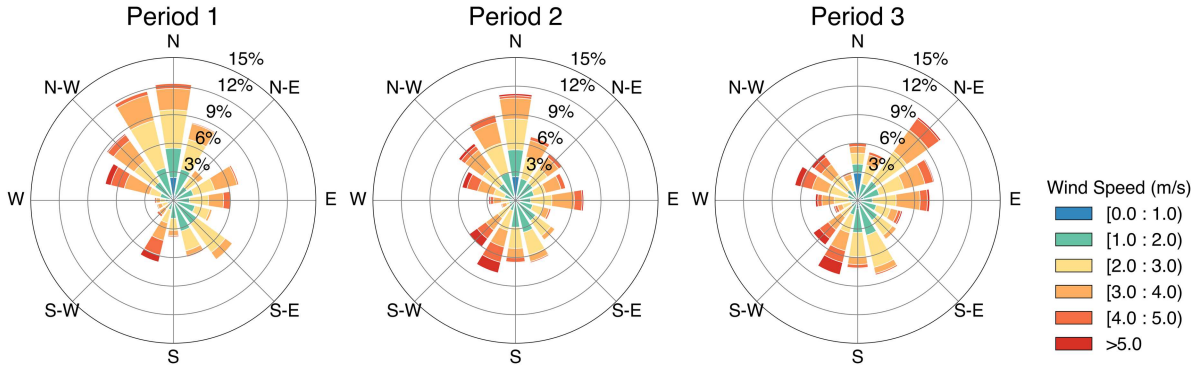

Figure 5. Wind rose plots for each period based on ASOS observations, showing the frequency distribution of wind direction and wind speed (m s^{-1}).

3.2 Tropospheric dominance index

As described in Section 2.7, enhanced TDI values reflect stronger NO_2 contributions from more distant locations along the SS viewing direction and are associated with satellite underestimation under high-NO_2 conditions. Therefore, in this section, satellite underestimation cases under high-NO_2 cases were separated using the TDI, defined as the ratio of $TrVCD_{SS}$ and $TrVCD_{DS}$ (see Section 2.6). To determine an appropriate threshold for separating high-TDI cases, we examined how the validation metrics change with different percentile thresholds (Figure A5). The correlation coefficient of the excluded high-TDI subset (TDI > threshold) increased when the threshold was lowered from the 95th to the 85th percentile, but showed almost no further change when the threshold was reduced from the 85th to the 80th percentile. This saturation indicates that the characteristic behavior of the high-TDI group is already sufficiently captured at the 85th percentile, and that further lowering the threshold does not meaningfully alter the composition of the excluded cases. Therefore, the 85th percentile (TDI = 1.10) was selected as the final threshold. Figure 6 and Table 2 summarize the results obtained after applying the 85th percentile threshold of the TDI to exclude high sub-pixel inhomogeneity cases. When the high TDI cases (TDI > 85th percentile) were excluded, the correlation coefficient slightly increased from 0.55 to 0.58, and the regression slope slightly increased from 0.74 to 0.80. The excluded high-TDI cases exhibited a pronounced negative bias, with an MD of -2.67×10^{15} molec. cm^{-2} and an MRD of −13.9%, indicating that GEMS underestimation cases were effectively separated. A similar effect was also observed in TROPOMI. When the high-TDI cases were excluded, the correlation coefficient improved from 0.78 to 0.83, and the regression slope increased from 0.66 to 0.75. In addition, the high-TDI cases showed negative MD (-3.28×10^{15} molec. cm^{-2}) and MRD (−29.4%), indicating that underestimation cases were effectively classified. Furthermore, the spatial distributions shown in Figure 6e, f reveal that NO_2 was more widely transported toward the observation site in the TDI > 85th percentile cases. In addition to enhanced spatial inhomogeneity, retrieval uncertainties in the a priori vertical profile (shape factor) may also contribute to the degraded agreement under high-TDI and high-NO_2 conditions. Because GEMS currently relies on monthly climatological profiles, errors in the assumed vertical distribution can increase when strong pollution plumes are present along the SS viewing direction. Thus, part of the improvement after excluding high-TDI cases may reflect a reduced influence of profile-related AMF errors, in addition to the intended screening of sub-pixel spatial inhomogeneity.

These findings support the interpretation that enhanced TDI values are linked to increased sub-pixel scale spatial inhomogeneity, which may not be fully captured by GEMS due to its coarse spatial resolution and averaging effect. This approach shows the potential of TDI as an auxiliary indicator for identifying sub-pixel inhomogeneity of NO_2 using the Pandora instrument. Nevertheless, further evaluation at different sites will be necessary to assess its general applicability.

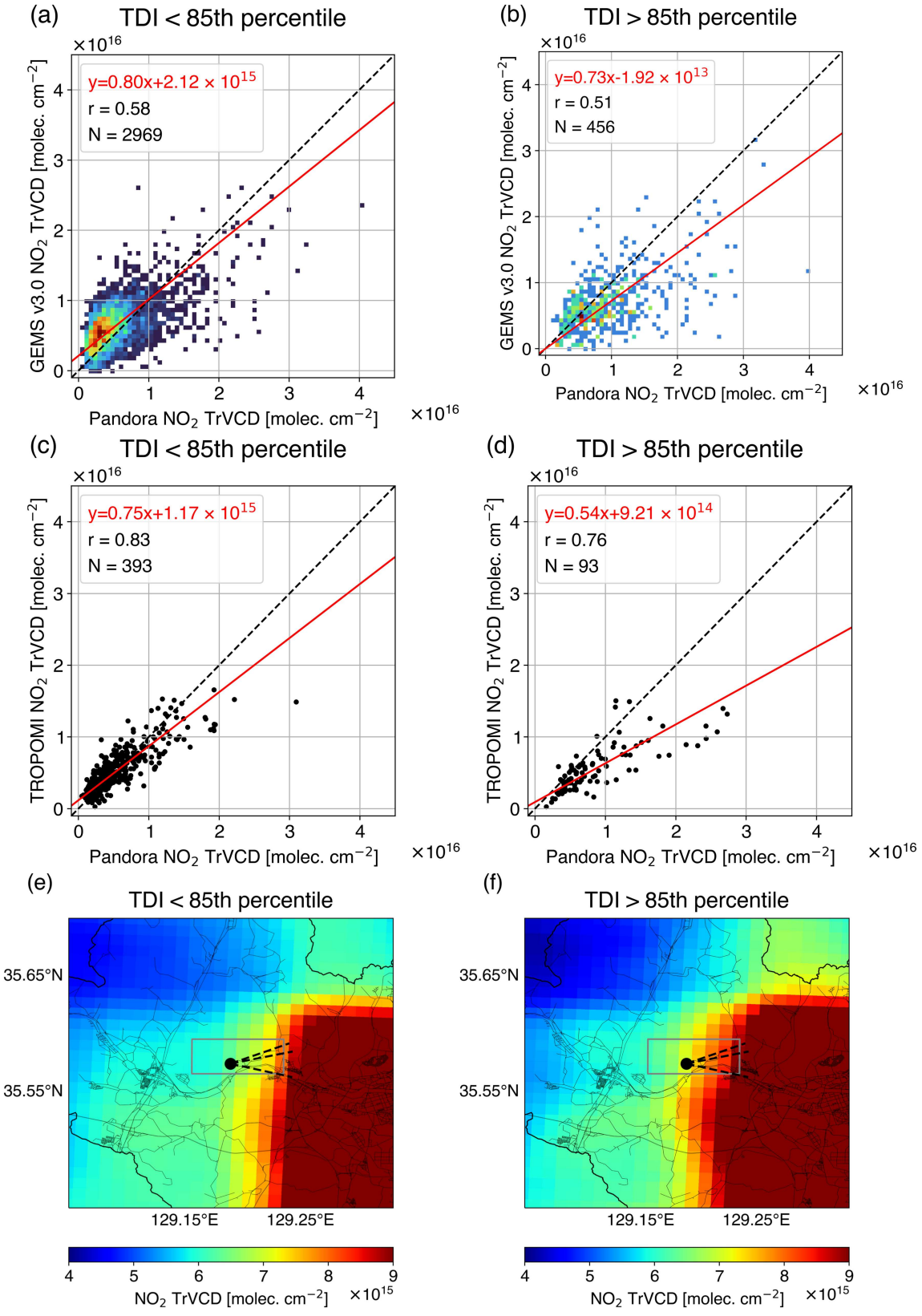

Figure 6. Comparison of satellite and Pandora NO_2 TrVCDs and corresponding GEMS distributions under different TDI conditions. Panels (a)–(b) compare GEMS with Pandora, (c)–(d) compare TROPOMI with Pandora, and (e)–(f) show the averaged GEMS NO_2 TrVCD maps for each condition. The red and black dashed lines in (a)–(d) indicate the regression and 1:1 lines, respectively. In (e)–(f), the black dot marks the P150 site, the dashed line denotes the SS-mode viewing direction, and the grey box indicates the co-located GEMS pixel.

3.3 Diurnal variation

Figure 7 shows the diurnal variation of NO_2 TrVCDs retrieved from GEMS and Pandora using the full dataset, separated by season. As discussed in Section 3.1, GEMS generally exhibited a positive bias compared to Pandora in all seasons except summer (JJA), which is also visible in Figure 7. In spring (MAM), the diurnal patterns of GEMS and Pandora were similar until 13:00 KST (Korean Standard Time), but after that, GEMS failed to capture the increase observed in Pandora. This late-afternoon increase is likely associated with strengthened southeasterly winds after noon, which transported polluted air masses from nearby industrial complexes toward the observation site. In summer (JJA), Pandora showed a generally flat diurnal pattern. Although southerly winds became stronger after 12:00 KST, potentially transporting NO_2 from industrial areas, high photochemical reactivity under strong solar radiation likely suppressed further accumulation, resulting in stable NO_2 levels during the afternoon. GEMS showed lower TrVCDs than Pandora during summer, particularly in the afternoon, which may be partly attributed to season-specific uncertainties, such as aerosol loading, surface reflectance, or cloud characteristics (Lin et al. 2015; Seo et al. 2024). Nevertheless, the number of coincident measurements in summer was relatively low compared to other seasons, which may limit the robustness of the statistics in this comparison. In autumn (SON) and winter (DJF), GEMS showed systematic bias, but the overall diurnal variation was similar between the two datasets. During autumn, NO_2 exhibited relatively flat diurnal patterns, with no prominent peak or dip throughout the day. However, both datasets showed a noticeable drop in NO_2 columns around 16:00 KST. The origin of this dip is unclear and should be interpreted carefully since the number of coincident measurements at that hour was relatively low compared to other times of the day. Additional data would be necessary to determine whether this feature reflects a real diurnal pattern or a sampling effect. Lastly, in winter, both instruments observed a slight increase in NO_2 columns throughout the day. This behavior is likely associated with the longer atmospheric lifetime of NO_2 under weak photochemical activity during the winter season, which allows for accumulation over time, as chemical loss is limited and wind speed and direction remain relatively constant throughout the day.

To investigate the influence of local transport on the diurnal pattern of NO_2 columns, wind directions were classified into two categories: polluted inflow (67.5° to 247.5°) and clean inflow (all other directions). Figure 8a illustrates the distribution of median NO_2 TrVCDs retrieved from Pandora as functions of wind direction and speed, based on ASOS observations. Higher NO_2 columns were generally observed under winds from the 67.5°-247.5° sector, which corresponds to the direction of major emission sources in Ulsan

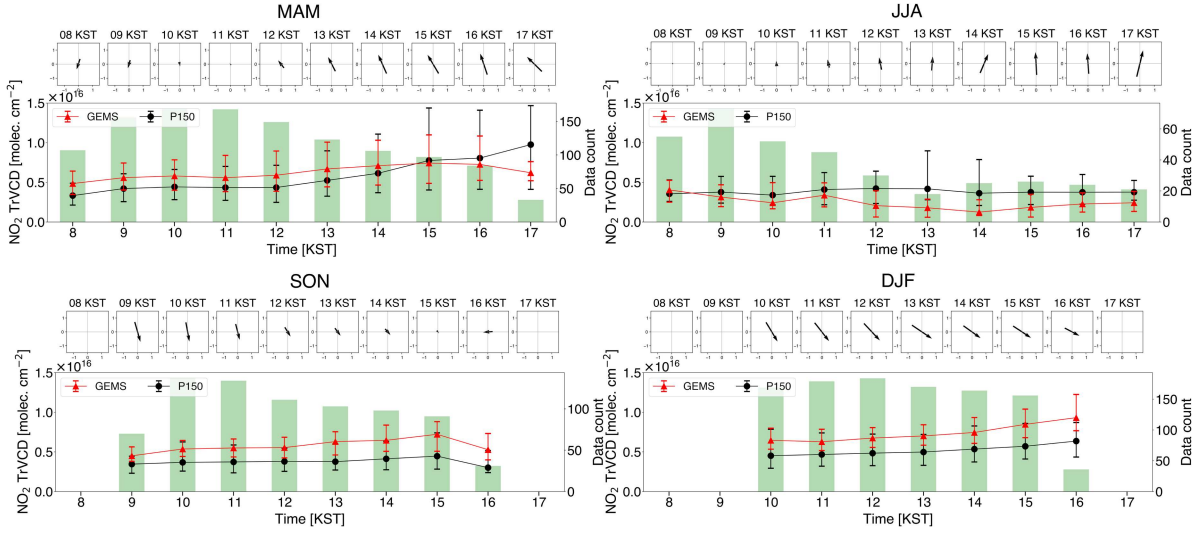

Figure 7. Diurnal variation in median NO_2 TrVCDs from P150 (black dot) and GEMS product (red triangle). Error bars represent the 25th and 75th percentiles of the Pandora and GEMS observations. Green bars represent the number of coincident measurements. Small vector plots above each panel indicate the hourly mean wind direction and speed based on ASOS observation data.

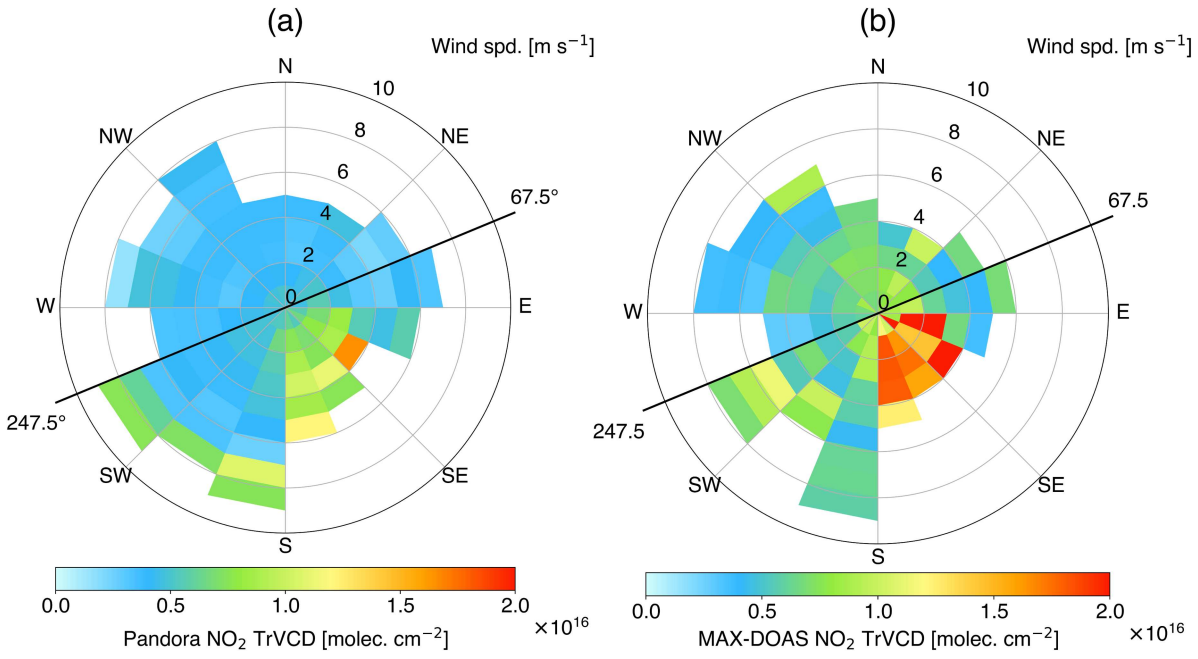

Figure 8. Wind-directional distribution of tropospheric NO_2 TrVCDs at (a) P150 and (b) MAX-DOAS stations (IUP-UB with 25° viewing direction and BIRA) as a function of wind direction and speed based on ASOS observations. Color represents median NO_2 TrVCD, radius represents wind speed.

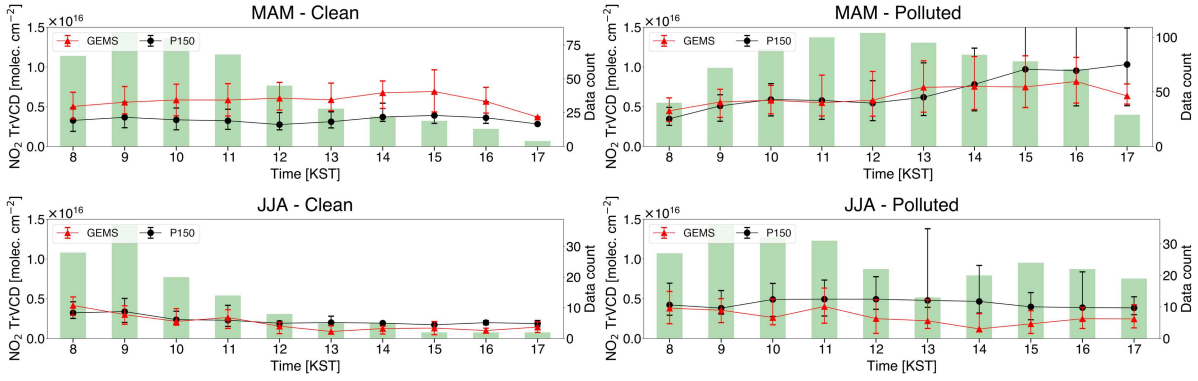

Figure 9. Same as Figure 5, but for clean inflow (left column) and polluted inflow (right column) conditions during spring (MAM) and summer (JJA).

(see Figure 1). This classification was used to examine the seasonal diurnal variation of NO_2 under different inflow conditions, particularly focusing on the discrepancies observed during spring and summer.

Figure 9 illustrates the diurnal patterns of NO_2 TrVCDs observed during spring (MAM) and summer (JJA), separated by polluted and clean inflow conditions. During both seasons, the diurnal variations under polluted inflow conditions exhibited a distinct discrepancy between Pandora and GEMS observations compared to those under clean inflow conditions. In spring, under clean inflow conditions, although GEMS showed a systematic positive bias, both GEMS and Pandora showed relatively flat diurnal patterns with no significant variation throughout the day. In contrast, under polluted inflow conditions, Pandora showed a more pronounced late-afternoon increase in NO_2 columns. Although GEMS also increased, the magnitude of the increase was smaller than that observed by Pandora.

In summer, although the number of observations under clean inflow conditions was limited, both instruments exhibited similar NO_2 levels and flat diurnal patterns. Under polluted inflow conditions,

Pandora maintained elevated NO_2 columns with little diurnal variation, whereas GEMS displayed a gradual decrease until 14:00 KST, followed by a slight rebound.

These results suggest that local transport contributes to the observed discrepancies in the diurnal patterns between satellite and ground-based measurements. However, transport alone does not fully account for the summertime disagreement. As shown in Figure 3, GEMS tends to underestimate NO_2 TrVCDs only during the summer season. This indicates the need for further investigation of season-specific retrieval uncertainties, such as surface reflectance and aerosol information used in the GEMS retrieval algorithm.

3.4 Comparison of GEMS NO_2 TrVCD and campaign instruments

Figure 10 shows the comparison results of GEMS NO_2 TrVCDs using MAX-DOAS observations at the IUP-UB site for four viewing azimuth angles (349°, 25°, 90°, and 145°) from June to October 2022. Each viewing direction points toward a suburban area (349°), the downtown district (25°), the petrochemical industrial complex (90°), and the Onsan industrial complex (145°). The wind speed is visualized by the color scale, and the corresponding statistical results are summarized in Table 3.

The average NO_2 TrVCDs retrieved from MAX-DOAS increased with the strength of emission sources in each direction, with the lowest value observed in the 349° direction (0.89×10^{16} molec. cm^{-2}), followed by 25° (1.07×10^{16} molec. cm^{-2}), and the highest values in the 90° and 145° directions (1.51×10^{16} and 1.61×10^{16} molec. cm^{-2}, respectively). This directional pattern suggests that, similar to the behavior observed at the P150 site, GEMS tends to show greater underestimation under high NO_2 columns when viewing directions are aligned with strong emission sources.

By combining IUP-UB data observed toward 25°, which is closely aligned with the viewing direction of the BIRA instrument (35°), the observational period was extended to June 2023 while accounting for the influence of MAX-DOAS viewing direction. The comparison results between GEMS and the combined MAX-DOAS dataset are shown in Figure 11, and the corresponding statistics are summarized in Table 4. The slope and correlation coefficient between GEMS and MAX-DOAS were 0.81 and 0.42, respectively. Recalling the validation result with Pandora during Period 2 (Section 3.1), the slope from the MAX-DOAS (0.81) comparison was similar to that of Pandora (0.79). However, the correlation coefficient from the merged MAX-DOAS dataset (0.42) was lower than that of Pandora (0.61). This discrepancy mainly originated from the behavior under high-NO_2 cases. When the NO_2 TrVCD was below 1×10^{16} molec. cm^{-2}, GEMS tended to overestimate the values, consistent with the results at P150. However, for values exceeding 1×10^{16} molec. cm^{-2}, GEMS occasionally overestimated, in contrast to the dominant underestimation trend observed at P150.

To investigate the cause of the weak correlation, the dataset was divided into clean (Figure 11b) and polluted (Figure 11c) conditions. Under clean inflow conditions, the agreement between GEMS and MAX-DOAS improved, with a slope of 1.06 and a correlation coefficient of 0.59, compared to a slope of 0.81 and a correlation coefficient of 0.33 under polluted inflow conditions. Furthermore, Figure A6 presents the results of categorizing the data into four groups by combining the polluted and clean inflow conditions and calm (<2 m s^{-1}) and windy (≥ 2 m s^{-1}) conditions. The 2 m s^{-1} threshold was determined based on the wind speed distribution observed by ASOS wind data (Figure A5) and previous atmospheric studies (Beirle et al. 2011; Liu et al. 2016). In both wind direction categories, calm conditions exhibited lower correlation coefficients than windy conditions. Notably, in the polluted inflow case, the correlation coefficient significantly decreased from 0.44 under windy conditions to 0.20 under calm conditions. This drop is much more pronounced than that observed at the Pandora site (0.65 under windy and 0.49 under calm conditions). Chan et al. (2020) reported that in Munich, higher wintertime wind speeds (~3.3 m s^{-1}) resulted in a more homogeneous distribution of NO_2, whereas lower summertime winds (~2.2 m s^{-1}) were associated with enhanced spatial variability. This finding supports our interpretation that under windy conditions, local inhomogeneities are smoothed out, thereby improving the agreement between GEMS and MAX-DOAS. Consequently, even within the same urban area, the characteristics of NO_2 may vary depending on the distribution of emission sources and the relative location of observation sites.

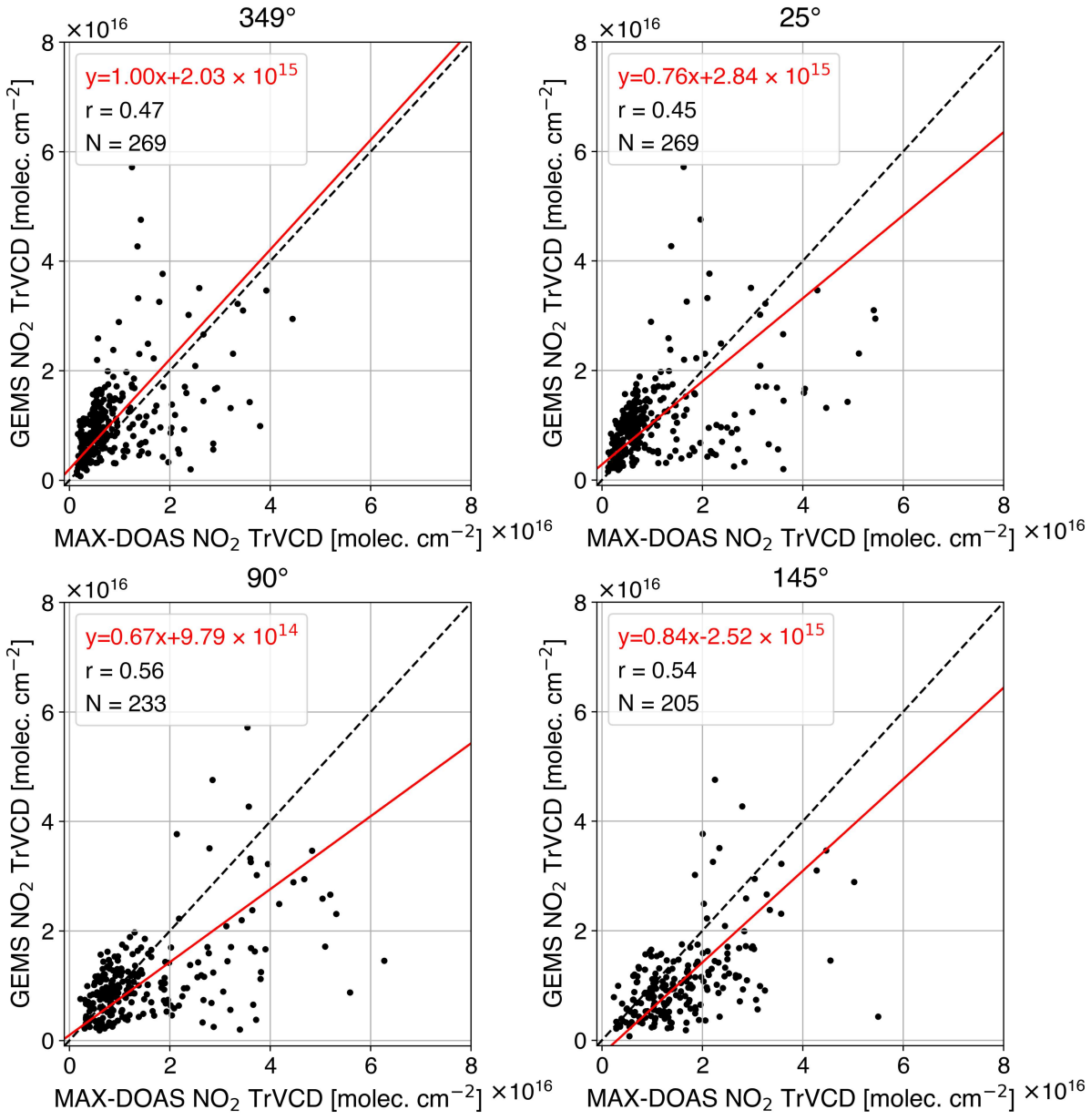

Figure 10. Scatter plots of MAX-DOAS (X-Axis) and GEMS (Y-Axis) NO_2 TrVCDs at IUP-UB station for different MAX-DOAS viewing directions. The color indicates the wind speed observed at the ASOS station.

Table 3. GEMS NO_2 TrVCD validation statistics at IUP-UB. The uncertainty of MD and MRD represents the standard error.

VAA	Slope[a]	y-intercept[b]	MD[c]	MAD[d]	MRD[e]	r[f]	n[g]
349°	1.00	2.03	2.05 ± 0.49	5.84 ± 0.35	61.0 ± 5.7	0.47	269
25°	0.76	2.84	0.26 ± 0.59	6.55 ± 0.43	46.3 ± 5.1	0.45	269
90°	0.67	0.98	−4.08 ± 0.65	7.11 ± 0.53	−6.5 ± 3.7	0.56	233
145°	0.84	−2.52	−5.15 ± 0.57	7.16 ± 0.45	−23.2 ± 3.3	0.54	205

[a]RMA regression slope.
[b]y-intercept of RMA regression (× 10^{15} molec. cm^{-2}).
[c]Mean difference (× 10^{15} molec. cm^{-2}).
[d]Mean absolute difference (× 10^{15} molec. cm^{-2}).
[e]Mean relative difference (%).
[f]Correlation coefficient.
[g]Number of coincident measurements.

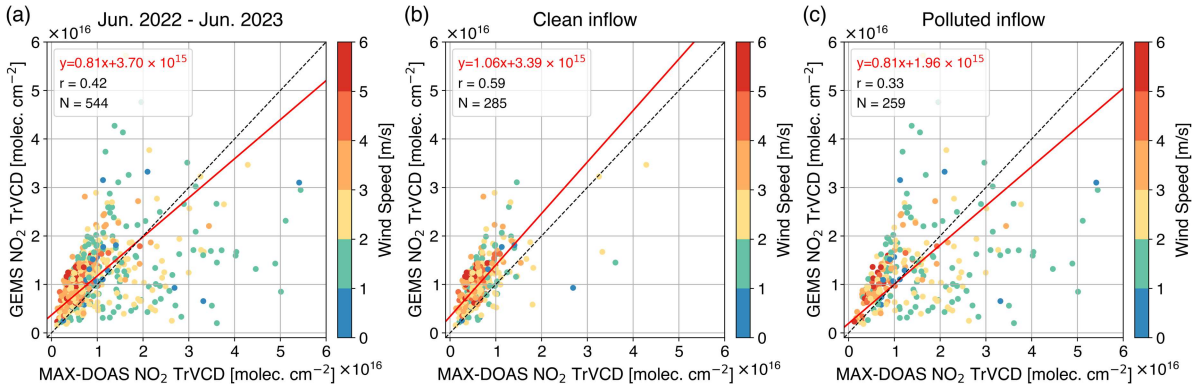

Figure 11. Scatter plots comparing NO_2 TrVCDs from MAX-DOAS (X-Axis) and GEMS (Y-Axis) at the IUP-UB (in the 25° azimuthal direction) and BIRA (in the 35° azimuthal direction) stations. The red solid lines indicate the regression lines, and the black dashed lines represent the 1:1 reference lines. The color scale in the panel shows wind speed.

Table 4. GEMS NO_2 TrVCD validation statistics at IUP-UB and BIRA station. The uncertainty of MD and MRD represents the standard error.

	Slope[a]	y-intercept[b]	MD[c]	MAD[d]	MRD[e]	r[f]	n[g]
All	0.81	3.70	1.68 ± 0.36	6.20 ± 0.26	50.1 ± 3.2	0.42	544
Clean	1.06	3.39	3.84 ± 0.27	4.72 ± 0.21	73.3 ± 4.2	0.59	285
Polluted	0.81	1.96	−0.70 ± 0.68	7.82 ± 0.47	25.6 ± 4.4	0.33	259

[a]RMA regression slope.
[b]y-intercept of RMA regression (× 10^{15} molec. cm^{-2}).
[c]Mean difference (× 10^{15} molec. cm^{-2}).
[d]Mean absolute difference (× 10^{15} molec. cm^{-2}).
[e]Mean relative difference (%).
[f]Correlation coefficient.
[g]Number of coincident measurements.

4 Summary and conclusion

In this study, the GEMS v3.0 NO_2 TrVCD product was evaluated over Ulsan, South Korea, using three years of Pandora observations (August 2021–July 2024) and campaign-based MAX-DOAS observations (June–October 2022 for IUP-Bremen and January–June 2023 for BIRA instrument). Compared with Pandora, GEMS exhibited fair agreement with a slope of 0.74, a correlation coefficient of 0.55, and a mean relative difference of +46%. Compared to the GEMS v2.0 performance (r = 0.51, slope = 0.62, MRD = +113%), the v3.0 retrievals showed a clear improvement in agreement and reduced bias. This indicates that algorithmic updates in v3.0, such as refined shape factors, updated tropopause pressure, and enhanced auxiliary products for AMF computation, have improved the retrieval performance. Year-to-year analysis revealed a performance decline in Period 3 (r = 0.44, slope = 0.66), which coincided with the change in Pandora viewing azimuth toward the industrial area and an increased frequency of polluted inflow from easterly and southerly directions.

The TDI, defined as the ratio between Pandora $TrVCD_{SS}$ and $TrVCD_{DS}$, proved useful as a diagnostic indicator of sub-pixel inhomogeneity. Excluding high-TDI cases (TDI > 1.10, 85th percentile) improved the slope from 0.74 to 0.80 and the correlation coefficient from 0.54 to 0.58, while the removed cases exhibited strong underestimation (MRD = −13.9% and MD = -2.67×10^{15} molec. cm^{-2}). A similar effect was also observed in TROPOMI. When the high-TDI cases were excluded, the correlation coefficient improved from 0.78 to 0.83, and the regression slope increased from 0.66 to 0.75. In addition, the high-TDI cases showed negative MD (-3.28×10^{15} molec. cm^{-2}) and MRD (−29.4%). This suggests that the TDI can serve as a useful auxiliary indicator for highly inhomogeneous conditions at the sub-pixel scale that are not fully resolved by GEMS at the UNIST site.

Seasonal analyses of diurnal variation further revealed that GEMS captured the general daily patterns in autumn and winter but failed to reproduce the late-afternoon increase in spring and showed a systematic underestimation in summer. These mismatches were pronounced under polluted inflow conditions, when industrial plumes were transported toward the observation site. These discrepancies likely reflect limitations in the a priori vertical profile shape factor, which in the current GEMS algorithm is based on monthly climatology and may not fully represent daily variability. The persistent summer underestimation suggests unresolved retrieval uncertainties associated with surface reflectance, aerosols, and cloud effects, underscoring the need for season-specific algorithm improvements.

During the SIJAQ2022 campaign, comparisons using MAX-DOAS near emission sources showed a slope of 0.81, a correlation coefficient of 0.42, and a mean relative difference of +51%. Agreement was notably better under clean inflow (slope = 1.06, r = 0.59) than under polluted inflow (slope = 0.81, r = 0.33) and degraded further under calm conditions (<2 m s^{-1}). These findings demonstrate that the meteorological conditions and site representativeness critically influence the consistency between satellite and ground-based observations.

Overall, this multi-year validation highlights both the progress and remaining challenges of the GEMS v3.0 retrievals. The algorithmic updates have improved the agreement with ground-based instruments, yet season-dependent biases remain evident, particularly in summer. This underscores the need for additional season-specific analyses to better characterize and mitigate retrieval uncertainties. The application of the TDI is expected to enhance the reliability of satellite-based NO_2 validation by providing a practical means to screen out highly inhomogeneous cases, thereby improving the interpretation of pixel-to-point comparison results. The applicability of the TDI may be limited in uniformly polluted regions or background areas where NO_2 is relatively homogeneously distributed. However, it is considered to be useful in regions such as Ulsan, where satellite observations underestimate high-NO_2 conditions due to localized emissions. It should also be noted that high-TDI conditions frequently coincide with elevated NO_2 levels, under which the climatological a priori vertical profiles used in the GEMS AMF calculation may become less representative. Consequently, part of the improvement obtained after excluding high-TDI cases may also reflect a reduced influence of profile-related AMF uncertainties, in addition to the intended screening of sub-pixel spatial inhomogeneity. In Korea, Busan is considered a potential site for application, as similar characteristics have been observed in previous studies (Lange et al. 2024; Bae et al. 2025). In future work, analyses will be conducted to evaluate the applicability of the TDI using long-term Pandora observations across multiple sites within the GEMS domain to further assess its applicability.

Acknowledgements

This work was supported by the National Research Foundation of Korea (NRF) grant funded by the Korea government Ministry of Science and ICT (MSIT) [RS−2025−00522393]; the Korea Environment Industry & Technology Institute (KEITI) through "Climate Change R&D Project for New Climate Regime" funded by the Korea Ministry of Environment (MOE) [Grant Number 2022003560002]; and the National Institute of Environment Research (NIER) funded by the Ministry of Environment (MOE) of the Republic of Korea [Grant Number NIER−2021−03−03−007). We thank the National Institute of Environmental Research of South Korea for providing GEMS level−2 data and the organization of the SIJAQ2022 field campaigns. We thank all participants of the SIJAQ2022 field campaign. We thank PGN support staff and funding for establishing and maintaining the Pandora sites used in this investigation. The PGN is a bilateral project supported with funding from NASA and ESA.

Author contributions

CRediT: **Kangho Bae**: Conceptualization, Methodology, Software, Investigation, Writing – Original Draft, Writing – Review & Editing; **Andreas Richter**: Investigation, Resources, Writing – Review & Editing; **Kezia Lange**: Investigation, Writing – Review & Editing; **Martina M. Friedrich**: Investigation, Data Curation, Formal analysis, Writing – Review & Editing; **Gaia Pinardi**: Formal analysis, Writing – Review & Editing; **Michel Van Roozendael**: Resources, Writing – Review & Editing; **Alexis Merlaud**: Investigation, Writing – Review & Editing; **Caroline Fayt**: Investigation, Data Curation; **Tim Bösch**: Investigation, Writing – Review & Editing; **Bianca Zilker**: Investigation; **Miriam Latsch**: Investigation; **Lisa K. Behrens**: Investigation; **Hanlim Lee**: Investigation, Data Curation; **Yeonjin Jung**: Writing –

Review & Editing, Data Curation; **Hyunkee Hong**: Project administration, Resources; **Lim-Seok Chang**: Project administration, Resources; **Chang-Keun Song:** Supervision**,** Resources, Writing – Review & Editing.

Disclosure statement

The authors declare that they have no known competing financial interests or personal relationships that could have appeared to influence the work reported in this paper.

ORCID

Kangho Bae 0000-0003-2216-2644
Andreas Richter 0000-0003-3339-212X
Kezia Lange 0000-0003-4435-3839
Martina M. Friedrich 0000-0002-4752-1837
Gaia Pinardi 0000-0001-5428-916X
Alexis Merlaud 0000-0002-5165-5504
Caroline Fayt 0009-0006-1560-6621
Tim Bösch 0000-0003-4230-8129
Miriam Latsch 0000-0002-3690-3178
Lisa K. Behrens 0000-0001-7081-8957
Hanlim Lee 0000-0002-4681-1269
Lim-Seok Chang 0000-0002-3296-546X
Chang-Keun Song 0000-0002-8987-2176

Data availability statement

GEMS L2 NO2 data can be accessed at https://nesc.nier.go.kr/en/html/cntnts/91/static/page.do (National Institute of Environmental Research, NIER, last access: 23 September 2025). The Pandora data are available from the PGN data archive (https://data.pandonia-global-network.org/, last access: 23 September 2025). The FRM4DOAS MAX-DOAS data are available on request. The codes that support the findings of this study are available at https://doi.org/10.7910/DVN/TGKIZ6.

References

Bae, K., C. -K. Song, M. Van Roozendael, A. Richter, T. Wagner, A. Merlaud, G. Pinardi, M. M. Friedrich, C. Fayt , and E. Dimitropoulou. 2025. "Validation of GEMS Operational v2. 0 Total Column NO2 and HCHO during the GMAP/SIJAQ Campaign." *Science of The Total Environment* 974: 179190. https://doi.org/10.1016/j.scitotenv.2025.179190.

Behera, S. N., and M. Sharma. 2011. "Degradation of SO2, NO2 and NH3 Leading to Formation of Secondary Inorganic Aerosols: An Environmental Chamber Study." *Atmospheric environment* 45(24): 4015–4024. https://doi.org/10.1016/j.atmosenv.2011.04.056.

Beirle, S., K. F. Boersma, U. Platt, M. G. Lawrence , and T. Wagner. 2011. "Megacity Emissions and Lifetimes of Nitrogen Oxides Probed from Space." *Science* 333(6050): 1737–1739. https://doi.org/10.1126/science.1207824.

Beirle, S., S. Dörner, S. Donner, J. Remmers, Y. Wang , and T. Wagner. 2019. "The Mainz Profile Algorithm (Mapa)." *Atmospheric Measurement Techniques* 12(3): 1785–1806. https://doi.org/10.5194/amt-12-1785-2019.

Bey, I., D. J. Jacob, R. M. Yantosca, J. A. Logan, B. D. Field, A. M. Fiore, Q. Li, H. Y. Liu, L. J. Mickley , and M. G. Schultz. 2001. "Global Modeling of Tropospheric Chemistry with Assimilated Meteorology: Model Description and Evaluation." *Journal of Geophysical Research: Atmospheres* 106(D19): 23073–23095. https://doi.org/10.1029/2001JD000807.

Boersma, K., D. Jacob, M. Trainic, Y. Rudich, I. DeSmedt, R. Dirksen , and H. Eskes. 2009. "Validation of Urban NO 2 Concentrations and Their Diurnal and Seasonal Variations Observed from the SCIAMACHY and OMI Sensors Using in Situ Surface Measurements in Israeli Cities." *Atmospheric Chemistry and Physics* 9(12): 3867–3879. https://doi.org/10.5194/acp-9-3867-2009.

Bovensmann, H., J. Burrows, M. Buchwitz, J. Frerick, S. Noel, V. Rozanov, K. Chance , and A. Goede. 1999. "SCIAMACHY: Mission Objectives and Measurement Modes." *Journal of the Atmospheric Sciences* 56(2): 127–150. https://doi.org/10.1175/1520-0469(1999)056<0127:SMOAMM>2.0.CO;2.

Burrows, J. P., M. Weber, M. Buchwitz, V. Rozanov, A. Ladstätter-Weißenmayer, A. Richter, R. DeBeek, R. Hoogen, K. Bramstedt , and K. -U. Eichmann. 1999. "The Global Ozone Monitoring Experiment (GOME): Mission Concept and First Scientific Results." *Journal of the Atmospheric Sciences* 56(2): 151–175. https://doi.org/10.1175/1520-0469(1999)056<0151:TGOMEG>2.0.CO;2.

Cede, A. 2024. "Manual for Blick Software Suite 1.8".

Chan, K. L., M. Wiegner, C. Alberti, and M. Wenig. 2020. "MAX-DOAS Measurements of Tropospheric NO 2 and HCHO in Munich and the Comparison to OMI and TROPOMI Satellite Observations." *Atmospheric Measurement Techniques Discussions* 2020: 1–31. https://doi.org/10.5194/amt-13-4499-2020.

Choi, Y., Y. Kanaya, H. Takashima, H. Irie, K. Park , and J. Chong. 2021. "Long-Term Variation in the Tropospheric Nitrogen Dioxide Vertical Column Density over Korea and Japan from the MAX-DOAS Network, 2007–2017." *Remote Sensing* 13(10): 1937. https://doi.org/10.3390/rs13101937.

Clarke, M. 1980. "The Reduced Major Axis of a Bivariate Sample." *Biometrika* 67(2): 441–446. https://doi.org/10.1093/biomet/67.2.441.

Crutzen, P. J. 1979. "The Role of NO and NO2 in the Chemistry of the Troposphere and Stratosphere." *Annual review of earth and planetary sciences* 7(1): 443–472. https://doi.org/10.1146/annurev.ea.07.050179.002303.

Danckaert, T., Fayt, C., Van Roozendael, M., Smedt, IDe, Letocart, V., Merlaud, A., and Pinardi, G. 2017. "QDOAS Software User Manual." http://uv-vis.aeronomie.be/software/QDOAS/QDOAS_manual.pdf.

de Foy, B., Z. Lu, D. G. Streets, L. N. Lamsal , and B. N. Duncan. 2015. "Estimates of Power Plant NOx Emissions and Lifetimes from OMI NO2 Satellite Retrievals." *Atmospheric environment* 116: 1–11. https://doi.org/10.1016/j.atmosenv.2015.05.056.

Edwards, D. P, S. Martínez-Alonso, D. S. Jo, I. Ortega, L. K. Emmons, J. J. Orlando, H. M. Worden, J. Kim, H. Lee, and J. Park. 2024. "Quantifying the Diurnal Variation of Atmospheric NO 2 from Observations of the Geostationary Environment Monitoring Spectrometer (Gems)." *EGUsphere* 2024: 1–31. https://doi.org/10.5194/acp-24-8943-2024.

Eskes, H, and Eichmann, K. 2023. "S5P MPC Product Readme Nitrogen Dioxide." https://sentinels.copernicus.eu/documents/247904/3541451/Sentinel-5P-Nitrogen-Dioxide-Level-2-Product-Readme-File.

Friedrich, M. M., C. Rivera, W. Stremme, Z. Ojeda, J. Arellano, A. Bezanilla, J. A. García-Reynoso , and M. Grutter. 2019. "NO 2 Vertical Profiles and Column Densities from MAX-DOAS Measurements in Mexico City." *Atmospheric Measurement Techniques* 12(4): 2545–2565. https://doi.org/10.5194/amt-12-2545-2019.

Gulde, S., M. Kolm, D. Smith, R. Maurer, G. B. Courrèges-Lacoste, M. Sallusti, and G. Bagnasco. 2017. Sentinel 4: A Geostationary Imaging UVN Spectrometer for Air Quality Monitoring: Status of Design, Performance and Development. *Paper presented at the International Conference on Space Optics—ICSO 2014*

Haagen-Smit, A. J. 1952. "Chemistry and Physiology of Los Angeles Smog." *Industrial Engineering Chemistry* 44(6): 1342–1346. https://doi.org/10.1021/ie50510a045.

Herman, J., A. Cede, E. Spinei, G. Mount, M. Tzortziou , and N. Abuhassan. 2009. "NO2 Column Amounts from Ground-Based Pandora and MFDOAS Spectrometers Using the Direct-Sun DOAS Technique: Intercomparisons and Application to OMI Validation." *Journal of Geophysical Research: Atmospheres* 114(D13). https://doi.org/10.1029/2009JD011848.

Herman, J., N. Abuhassan, J. Kim, J. Kim, M. Dubey, M. Raponi , and M. Tzortziou. 2019. "Underestimation of Column NO 2 Amounts from the OMI Satellite Compared to Diurnally Varying Ground-Based Retrievals from Multiple PANDORA Spectrometer Instruments." *Atmospheric Measurement Techniques* 12(10): 5593–5612. https://doi.org/10.5194/amt-12-5593-2019.

Ialongo, I., H. Virta, H. Eskes, J. Hovila , and J. Douros. 2020. "Comparison of TROPOMI/Sentinel-5 Precursor NO 2 Observations with Ground-Based Measurements in Helsinki." *Atmospheric Measurement Techniques* 13(1): 205–218. https://doi.org/10.5194/amt-13-205-2020.

Irie, H., H. Takashima, Y. Kanaya, K. F. Boersma, L. Gast, F. Wittrock, D. Brunner, Y. Zhou , and M. Van Roozendael. 2011. "Eight-Component Retrievals from Ground-Based MAX-DOAS Observations." *Atmos. Meas. Tech.* 4(6): 1027–1044. https://doi.org/10.5194/amt-4-1027-2011.

Jarraud, M. 2008. Guide to Meteorological Instruments and Methods of Observation (WMO-No. 8). Geneva, Switzerland: World Meteorological Organisation, 29.

Judd, L. M., J. A. Al-Saadi, S. J. Janz, M. G. Kowalewski, R. B. Pierce, J. J. Szykman, L. C. Valin, et al. 2019. "Evaluating the Impact of Spatial Resolution on Tropospheric NO2 Column Comparisons Within Urban Areas Using High-Resolution Airborne Data." *Atmos. Meas. Tech.* 12(11): 6091–6111. https://doi.org/10.5194/amt-12-6091-2019.

Judd, L. M., J. A. Al-Saadi, J. J. Szykman, L. C. Valin, S. J. Janz, M. G. Kowalewski, H. J. Eskes, J. P. Veefkind, A. Cede , and M. Mueller. 2020. "Evaluating Sentinel-5P TROPOMI Tropospheric NO 2 Column Densities with Airborne and Pandora Spectrometers Near New York City and Long Island Sound." *Atmospheric Measurement Techniques* 13(11): 6113–6140. https://doi.org/10.5194/amt-13-6113-2020.

Karagkiozidis, D., M. -E. Koukouli, A. Bais, D. Balis , and P. Tzoumaka. 2023. "Assessment of the NO2 Spatio-Temporal Variability over Thessaloniki, Greece, Using MAX-DOAS Measurements and Comparison with S5P/TROPOMI Observations." *Applied Sciences* 13(4): 2641. https://doi.org/10.3390/app13042641.

Kim, S. -J., H. -Y. Lee, S. -J. Lee , and S. -D. Choi. 2023b. "Passive Air Sampling of VOCs, O3, NO2, and SO2 in the Large Industrial City of Ulsan, South Korea: spatial–Temporal Variations, Source Identification, and Ozone Formation Potential." *Environmental Science and Pollution Research* 30(60): 125478–125491. https://doi.org/10.1007/s11356-023-31109-z.

Kim, H. C., S. Kim, S. -H. Lee, B. -U. Kim , and P. Lee. 2020a. "Fine-Scale Columnar and Surface NOx Concentrations over South Korea: Comparison of Surface Monitors, TROPOMI, CMAQ and CAPSS Inventory." *Atmosphere* 11(1): 101. https://doi.org/10.3390/atmos11010101.

Kim, J., U. Jeong, M. -H. Ahn, J. H. Kim, R. J. Park, H. Lee, C. H. Song, Y. -S. Choi, K. -H. Lee , and J. -M. Yoo. 2020b. "New Era of Air Quality Monitoring from Space: Geostationary Environment Monitoring Spectrometer (Gems)." *Bulletin of the American Meteorological Society* 101(1): E1–E22. https://doi.org/10.1175/BAMS-D-18-0013.1.

Kim, S., D. Kim, H. Hong, L. -S. Chang, H. Lee, D. -R. Kim, D. Kim, J. -A. Yu, D. Lee , and U. Jeong. 2023a. "First-Time Comparison between NO 2 Vertical Columns from GEMS and Pandora Measurements." *Atmospheric Measurement Techniques Discussions* 2023: 1–22.

Lamarque, J. -F., T. C. Bond, V. Eyring, C. Granier, A. Heil, Z. Klimont, D. Lee, C. Liousse, A. Mieville , and B. Owen. 2010. "Historical (1850–2000) Gridded Anthropogenic and Biomass Burning Emissions of Reactive Gases and Aerosols: Methodology and Application." *Atmospheric Chemistry and Physics* 10(15): 7017–7039. https://doi.org/10.5194/acp-10-7017-2010.

Lange, K., A Richter, T. Bösch, B. Zilker, M Latsch, L. K Behrens, C. M. Okafor, H. Bösch, J. P. Burrows, and A. Merlaud. 2024. "Validation of GEMS Tropospheric NO 2 Columns and Their Diurnal Variation with Ground-Based DOAS Measurements." *EGUsphere* 2024: 1–42.

Laughner, J. L. , and R. C. Cohen. 2019. "Direct Observation of Changing NO X Lifetime in North American Cities." *Science* 366(6466): 723–727. https://doi.org/10.1126/science.aax6832.

Lee, H., Park, J., Jung, Y., and Hong, H. 2024. Geostationary Environment Monitoring Spectrometer (GEMS) Algorithm Theoretical Basis Document, NO2 Retrieval Algorithm, Tech. rep., Environmental Satellite Center, National Institute of Environmental Research, Ministry of Environment, Issue 3.0 (last access: 23 September 2025). https://nesc.nier.go.kr/en/html/satellite/doc/doc.do.

Lee, S. -J., H. -Y. Lee, S. -J. Kim, H. -J. Kang, H. Kim, Y. -K. Seo, H. -J. Shin, Y. S. Ghim, C. -K. Song , and S. -D. Choi. 2023. "Pollution Characteristics of PM2. 5 during High Concentration Periods in Summer and Winter in Ulsan, the Largest Industrial City in South Korea." *Atmospheric environment* 292: 119418. https://doi.org/10.1016/j.atmosenv.2022.119418.

Levelt, P. F., G. H. Van Den Oord, M. R. Dobber, A. Malkki, H. Visser, JDe Vries, P. Stammes, J. O. Lundell, and H. Saari. 2006. "The Ozone Monitoring Instrument." *IEEE Transactions on geoscience and remote sensing* 44(5): 1093–1101.

Lin, J. -T., M. -Y. Liu, J. -Y. Xin, K. Boersma, R. Spurr, R. Martin , and Q. Zhang. 2015. "Influence of Aerosols and Surface Reflectance on Satellite NO 2 Retrieval: Seasonal and Spatial Characteristics and Implications for NO X Emission Constraints." *Atmospheric Chemistry and Physics* 15(19): 11217–11241. https://doi.org/10.5194/acp-15-11217-2015.

Liu, F., S. Beirle, Q. Zhang, S. Dörner, K. He , and T. Wagner. 2016. "NO X Lifetimes and Emissions of Cities and Power Plants in Polluted Background Estimated By Satellite Observations." *Atmospheric Chemistry and Physics* 16(8): 5283–5298. https://doi.org/10.5194/acp-16-5283-2016.

Madronich, S., B. Sulzberger, J. Longstreth, T. Schikowski, M. S. Andersen, K. Solomon , and S. Wilson. 2023. "Changes in Tropospheric Air Quality Related to the Protection of Stratospheric Ozone in a Changing Climate." *Photochemical Photobiological Sciences* 22(5): 1129–1176. https://doi.org/10.1007/s43630-023-00369-6.

Meng, X., C. Liu, R. Chen, F. Sera, A. M. Vicedo-Cabrera, A. Milojevic, Y. Guo, S. Tong, MdSZS Coelho, and P. H. N. Saldiva. 2021. "Short Term Associations of Ambient Nitrogen Dioxide with Daily Total, Cardiovascular, and Respiratory Mortality: Multilocation Analysis in 398 Cities." *bmj*, 372.

Munro, R., M. Eisinger, C. Anderson, J. Callies, E. Corpaccioli, R. Lang, A. Lefebvre, Y. Livschitz , and A. P. Albinana. 2006. "GOME-2 on Metop. *Paper presented at the Proc. of The 2006 EUMETSAT Meteorological Satellite Conference*. Helsinki, Finland.

Orellano, P., J. Reynoso, N. Quaranta, A. Bardach, and A. Ciapponi. 2020. "Short-term exposure to particulate matter (PM10 and PM2. 5), nitrogen dioxide (NO2), and ozone (O3) and all-cause and cause-specific mortality: Systematic review and meta-analysis." *Environment International* 142: 105876. https://doi.org/10.1016/j.envint.2020.105876.

Platt, U. and J. Stutz. 2008. *Differential absorption spectroscopy*. Berlin, Heidelberg: Springer.

Seinfeld, J. H. and S. N. Pandis. 2016. *Atmospheric Chemistry and Physics: from Air Pollution to Climate Change*. Hoboken, New Jersey: John Wiley & Sons.

Seo, S., P. Valks, R. Lutz, K. -P. Heue, P. Hedelt, V. Molina García, D. Loyola, H. Lee , and J. Kim. 2024. "Tropospheric NO2 Retrieval Algorithm for Geostationary Satellite Instruments: Applications to Gems." *Atmospheric Measurement Techniques* 17(20): 6163–6191. https://doi.org/10.5194/amt-17-6163-2024.

Spurr, R. J. 2006. "VLIDORT: A Linearized Pseudo-Spherical Vector Discrete Ordinate Radiative Transfer Code for Forward Model and Retrieval Studies in Multilayer Multiple Scattering Media." *Journal of Quantitative Spectroscopy and Radiative Transfer* 102(2): 316–342. https://doi.org/10.1016/j.jqsrt.2006.05.005.

Tilstra, L. G., M. de Graaf, V. J. H. Trees, P. Litvinov, O. Dubovik , and P. Stammes. 2024. "A Directional Surface Reflectance Climatology Determined from TROPOMI Observations." *Atmos. Meas. Tech.* 17(7): 2235–2256. https://doi.org/10.5194/amt-17-2235-2024.

Tirpitz, J. L., U. Frieß, F. Hendrick, C. Alberti, M. Allaart, A. Apituley, A. Bais, et al. 2021. "Intercomparison of MAX-DOAS Vertical Profile Retrieval Algorithms: Studies on Field Data from the CINDI-2 Campaign." *Atmos. Meas. Tech.* 14(1): 1–35. https://doi.org/10.5194/amt-14-1-2021.

van Geffen, J., H. Eskes, S. Compernolle, G. Pinardi, T. Verhoelst, J-C. Lambert, M. Sneep, M. ter Linden, A. Ludewig, K. F. Boersma, and J. P. Veefkind. 2022. "Sentinel-5P TROPOMI NO $_2$ retrieval: impact of version v2.2 improvements and comparisons with OMI and ground-based data." Atmospheric Measurement Techniques 15(7): 2037–2060. 2037-2060. os.enk. 10.5194/amt-15-2037-2022.

Van Roozendael, M., F. Hendrick, M. M. Friedrich, C. Fayt, A. Bais, S. Beirle, T. Bösch, M. Navarro Comas, U. Friess , and D. Karagkiozidis. 2024. "Fiducial Reference Measurements for Air Quality Monitoring Using Ground-Based MAX-DOAS Instruments (Frm4doas)." *Remote Sensing* 16(23): 4523. https://doi.org/10.3390/rs16234523.

Veefkind, J. P., I. Aben, K. McMullan, H. Förster, J. De Vries, G. Otter, J. Claas, H. Eskes, J. De Haan , and Q. Kleipool. 2012. "TROPOMI on the ESA Sentinel-5 Precursor: a GMES Mission for Global Observations of the Atmospheric Composition for Climate, Air Quality and Ozone Layer Applications." *Remote sensing of environment* 120: 70–83. https://doi.org/10.1016/j.rse.2011.09.027.

Verhoelst, T., S. Compernolle, G. Pinardi, J. -C. Lambert, H. J. Eskes, K. -U. Eichmann, A. M. Fjæraa, J. Granville, S. Niemeijer , and A. Cede. 2021. "Ground-Based Validation of the Copernicus Sentinel-5P TROPOMI NO 2 Measurements with the NDACC ZSL-DOAS, MAX-DOAS and Pandonia Global Networks." *Atmospheric Measurement Techniques* 14(1): 481–510. https://doi.org/10.5194/amt-14-481-2021.

Vlemmix, T., A. Piters, P. Stammes, P. Wang , and P. Levelt. 2010. "Retrieval of Tropospheric NO 2 Using the MAX-DOAS Method Combined with Relative Intensity Measurements for Aerosol Correction." *Atmospheric Measurement Techniques* 3(5): 1287–1305. https://doi.org/10.5194/amt-3-1287-2010.

Zhao, X., D. Griffin, V. Fioletov, C. McLinden, J. Davies, A. Ogyu, S. C. Lee, A. Lupu, M. D. Moran , and A. Cede. 2019. "Retrieval of Total Column and Surface NO 2 from Pandora Zenith-Sky Measurements." *Atmospheric Chemistry and Physics* 19(16): 10619–10642. https://doi.org/10.5194/acp-19-10619-2019.

Zoogman, P., X. Liu, R. Suleiman, W. Pennington, D. Flittner, J. Al-Saadi, B. Hilton, D. Nicks, M. Newchurch , and J. Carr. 2017. "Tropospheric Emissions: Monitoring of Pollution (Tempo)." *Journal of Quantitative Spectroscopy and Radiative Transfer* 186: 17–39. https://doi.org/10.1016/j.jqsrt.2016.05.008.